**Title**

Prefrontal neurocardiac networks during approach-avoidance behaviors



**ISBN**

9798293851515

**Author**

Mateo Semidey, Gabriel

**Publication Date**

2025-09-19

Peer reviewed|Thesis/dissertation

# Prefrontal neurocardiac networks during approach-avoidance behaviors

by
Gabriel Enrique Mateo Semidey

DISSERTATION
Submitted in partial satisfaction of the requirements for degree of
DOCTOR OF PHILOSOPHY

in

Neuroscience

in the

GRADUATE DIVISION
of the
UNIVERSITY OF CALIFORNIA, SAN FRANCISCO

Approved:

DocuSigned by:
Allan Basbaum
167A1C692498488...

Allan Basbaum
Chair

DocuSigned by:
Zachary Knight
[illegible]

Zachary Knight

DocuSigned by:
Vikaas Sohal
[illegible]

Vikaas Sohal

DocuSigned by:
[illegible]
D52190F39543433...

Mazen Kheirbek

Committee Members

## Acknowledgements

I would like to thank the advisors who have guided me throughout my scientific career: Carlos Gonzalez (University of Puerto Rico, Rio Piedras), Guillermo Yudowski (University of Puerto Rico, Institute of Neurobiology), Marisela Morales (National Insitute on Drug Abuse, NIH), and Vikaas Sohal (University of California, San Francisco).

I am deeply thankful to my friends, my mother Myrna, my father Juan, my brothers Juan and Pedro, my grandparents, and my partner Sahila for their love and support.

This work was supported by the National Institute of Mental Health (NIH).

**Prefrontal neurocardiac networks during approach-avoidance behaviors**

Gabriel Enrique Mateo Semidey

## ABSTRACT

Animals engage in approach-avoidance behaviors when confronted with potentially threatening cues. These behaviors are supported by neural computations and peripheral reactions in the body, such as autonomic signals that give rise to the classic “fight-or-flight” response. Significant changes in heart rate during these situations are a hallmark of this response. Importantly, the brain exerts top-down control over cardiac activity and heart rate can also influence brain function. Fluctuations in heart rate modulate neural activity in the medial prefrontal cortex (mPFC), a region involved in evaluating social environments, anxiogenic contexts, and guiding adaptive decisions. However, how cardiac signals are mapped in the mPFC during approach-avoidance behaviors remains unclear. To address this, we developed a multidisciplinary approach to simultaneously record heart rate and measure single-cell calcium signals from mPFC neurons in freely moving mice navigating social and anxiogenic contexts. This approach revealed neural ensembles in the mPFC that encode heart rate, which we termed “neurocardiac networks.” We hypothesized that activity in these neurons would decouple from heart rate in anxiogenic or social contexts that promote avoidance because the mPFC may prioritize threat evaluation or decision-making over interoceptive monitoring. Indeed, neurocardiac networks became decoupled when mice approached an aggressive mouse, but not a juvenile mouse. Moreover, decoupling increased when mice navigated environments thought to induce higher anxiety levels. Our findings provide a new framework for identifying functionally distinct neurons in the

mPFC using heart rate as a physiological readout, advancing our mechanistic understanding of how brain-heart interactions shape social and anxiety-related behaviors.

## TABLE OF CONTENTS

## LIST OF FIGURES

## LIST OF ABBREVIATIONS

AP: anterior-posterior

BLA: basolateral amygdala

BMA: basomedial amygdala

D2R: D2 receptor

DV: dorsal-ventral

ECG: electrocardiography

EPM: elevated plus maze

GRIN: gradient refractive index

HEP: heartbeat-evoked potential

+HR: +Heart Rate

-HR: -Heart Rate

HRV: heart rate variability

IDPS: Inscopix Data Processing Software

i.p.: intraperitoneal

iso: isoproterenol

ML: medial-lateral

mPFC: medial prefrontal cortex

NOE: novel object exploration

NTS: nucleus of the solitary tract

PFA: paraformaldehyde

PV: parvalbumin

VIP: vasoactive intestinal peptide

vmPFC: ventromedial portion of the mPFC

# Chapter 1 – General Introduction

## 1.1 Brain-heart interaction in emotions

Since the beginnings of the Egyptian civilization, the localization of emotions in the body has been widely debated.[1] This ancient question influenced the emergence of the cardiocentric and the cephalocentric theories, which proposed the heart or the brain as the source of emotions in the body.[1] While the cardiocentric theory suggested that the heart was the center of emotions, the cephalocentric theory suggested the brain as the producer of emotions.[1] The cardiocentric view was supported by the observation that emotions usually resulted in significant changes in heart rate,[2] whereas the cephalocentric view was reinforced by the fact that brain injuries could alter emotional experiences.[1] Despite this philosophical dichotomy, the cardiocentric view prevailed for centuries.

In the late 19th century, William James and Carl Lange proposed the James-Lange theory of emotion, which suggested that physiological reactions in the body (e.g. elevated heart rate) trigger emotional responses, rather than the opposite direction of causality.[3,4] But with advancements in neuroscience and psychology in the 20th century, the neurocentric view gained general acceptance in the medical and scientific community. This influenced the emergence of the Cannon-Bard theory and the Schachter-Singer Two-Factor theory of emotions. The Cannon-Bard theory suggested that emotions and physiological reactions in the body (e.g. elevated heart rate) occur simultaneously as the thalamus send signals to the cortex and the autonomic nervous system to produce a conscious emotional experience and a bodily reaction,

respectively.[5] The Schachter – Singer theory proposed that emotional responses are comprised of physiological and cognitive factors. Therefore, according to the Schachter-Singer theory the physiological reaction in the body is integrated in the brain and a valence-related label for such bodily reaction is assigned based on the context.[6] These views were followed by a series of refined hypothesis of emotions that resulted in the theories that are most accepted today: Ledoux's Dual Pathway theory and the theory of constructed emotion.

The theory of constructed emotion argue that emotions are not hardwired but constructed by the brain through sensory inputs, bodily signals, and past experiences.[7] In the context of the brain-heart interaction, this theory suggests that the brain integrates the cardiac signals with past experiences and the current environment to construct an initial emotional state, which it continuously updates as new information becomes available. Ledoux's Dual Pathway theory explains that emotions are processed through a "low road pathway" (i.e., fast and unconscious) and a "high road pathway" (i.e., slow and conscious)[8]. In the context of the brain-heart interaction, the low road pathway results in the recruitment of amygdala pathways that cause a fast emotional response and modulation of heart rate before conscious awareness, whereas the high road pathway results in the recruitment of cortico-amygdalar pathways through which the cortex integrates stimuli and produces a more controlled emotional response and bodily reaction.[8] In both theories, the cortex plays a crucial role in the integration of cardiac signals and the modulation of the emotional response.

## 1.2 Encoding and modulation of cardiac signals in the mPFC

The medial prefrontal cortex (mPFC) is a higher-order brain region capable of integrating cardiac signals and modulating autonomic function.[9-11] With each beat, the heart sends a series of cardiac signals that ascends through the autonomic nervous system, reaching the brainstem. Within the brainstem, the nucleus of the solitary tract (NTS) integrates and relays these cardiac signals to subcortical regions such as the hypothalamus and the amygdala, which are involved in autonomic regulation.[12-13] These subcortical regions subsequently transmit cardiac-related signals to the mPFC, where they undergo higher-order processing.[14-16]

Upon receiving cardiac-related signals, the mPFC processes this information in many ways. For example, the mPFC exhibits heartbeat-evoked potentials (HEPs), electrophysiological responses that are time-locked to individual heartbeats.[17,18] These evoked potentials reflect the integration and representation of cardiac signals within the mPFC, and may play a role in shaping autonomic regulation and decision making. Previous studies with combined magnetoencephalography and electrocardiography (ECG) in humans exposed to a visual task have demonstrated that HEPs in the mPFC before a visual stimulus onset predicts visual detection, and heart rate decreases more after the subject reported seeing the visual stimulus.[19]

Additional neuroimaging studies have shown that the mPFC exhibits activity patterns synchronized with the variation in time intervals between heartbeats (also known as heart rate variability or HRV).[20] A critical aspect of this regulation lies in the

interconnection between the mPFC and the amygdala. The strength of mPFC-amygdala connectivity has been linked to HRV, with stronger functional coupling associated with higher HRV and weaker functional coupling associated with reduced HRV.[20] This suggests that when the mPFC effectively communicates with amygdala, it can flexibly regulate amygdala-driven autonomic output, allowing for adaptive cardiovascular responses and high HRV. Conversely, a reduced mPFC-amygdala connectivity correlates the loss of this dynamic regulation, resulting in the autonomic alterations that are commonly present in stress- and anxiety-related disorders. In addition to top-down regulation, fluctuations in HRV may enhance o diminish the capacity of the mPFC-amygdala pathway to monitor and regulate bodily states, influencing attention, emotional regulation, and decision-making.

The role of the mPFC in modulating cardiac function has been explored through anatomic, genetic, pharmacologic, and optogenetic studies. Anatomic studies have demonstrated that the mPFC sends direct neural projections to brain regions which modulate the heart rate (such as the amygdala, hypothalamus, and the NTS).[21-24] Genetic knockdown of glutamate release from neurons in the infralimbic portion of the mPFC has been shown to enhance stress-induced elevations in heart rate.[25] Microinjection of L-glutamate in the ventral portion of the mPFC (mainly infralimbic cortex) elicits long-lasting tachycardic responses.[26] Moreover, optogenetic stimulation of neural projections from the ventromedial portion of the mPFC (vmPFC) to the basomedial amygdala (BMA) suppresses the elevation in heart rate that normally occur in anxiety-provoking environments.[10] Together, these findings highlight the importance

of the mPFC in the top-down control of cardiac states, and position the mPFC as a neural node with the capability to simultaneously monitor and modulate heart rate.

### 1.3 Encoding of social information in the mPFC

Social behaviors have played a major role in the evolution of many species and these behaviors can be advantageous or costly depending on the contextual valence. To navigate shifting social landscapes, animals must continuously evaluate the potential risks and rewards of engaging with others. This evaluation process is supported by neural circuits that integrate environmental cues, internal states, and prior experiences to shape appropriate behavioral responses. In recent years, growing attention has been paid to how these circuits modulate social decision-making, particularly in emotionally-salient contexts such as dominance hierarchies or threat encounters. Among the brain regions implicated in this process, the mPFC plays a pivotal role in evaluating social context and guiding adaptive behavioral responses.[27,28] The mPFC integrates sensory information with internal affective states, enabling flexible decision-making based on the perceived valence of a social interaction.[27,28] It is particularly important for encoding the value of social stimuli and exerting top-down control over subcortical structures involved in emotional reactivity, such as the amygdala.[27]

Dysregulation of mPFC activity has been linked to impaired social cognition.[29,30] For example, lesion studies have provided evidence for the critical role of the mPFC in regulating social behavior. Animals with mPFC lesions exhibit deficits in social cognition, including impaired social recognition and social interaction.[27,31] These

findings suggest that the mPFC is essential for processing social cues to recognize familiar individuals and engage in appropriate social interactions. In addition to lesion studies, genetic manipulations targeting the mPFC have further elucidated its role in social behavior. Disruption of genes implicated in synaptic function, neuronal excitability, or modulatory signaling results in social impairments. Mutations in the mPFC in genes associated with autism spectrum disorder, such as *Shank3* or *Cntnap2*, lead to reduced social interaction and abnormal social preference in rodents.[32,33] Complementing lesion and genetic studies, optogenetic manipulations have provided causal evidence for the dynamic role of the mPFC in modulating social interactions. Optogenetic activation or inhibition of specific neural subpopulation within the mPFC have demonstrated that prefrontal activity can bidirectionally influence social behavior.[33] For instance, optogenetic activation of parvalbumin (PV) interneurons or optogenetic inhibition of excitatory neurons in the mPFC rescue deficits in social behaviors in normal mice and in a mouse model of autism (*CNTNAP2* knockout mice).[33,34] Furthermore, optogenetic manipulations of mPFC projections to regions such as the amygdala, and periaqueductal gray contribute to various aspects of social behavior, including social interaction, and social avoidance.[35,36] Moreover, optogenetic excitation or inhibition of mPFC D2R+ neurons disrupt or enhances social interaction, respectively.[37] These findings underscore the role of the mPFC as a hub that integrates contextual and affective information to regulate social interactions.

Building on these experiments using causal manipulations, single-unit electrophysiology studies in rodents have shown that specific subpopulations of mPFC neurons are

selectively activated during presentation of social sensory cues.[38] These neurons often display a temporally structured activity that is tightly aligned to discrete social events, suggesting a role in encoding the salience and context of social stimuli. Moreover, neural ensemble analyses from calcium imaging studies have also demonstrated that social behavior is associated with coordinated activity patterns across mPFC neural populations, where correlated activity within mPFC neural ensembles is diminished in mice lacking the autism-associated gene *Shank3*.[39] These findings point to highly specialized and adaptable neural computations within the mPFC and underlies its capability to guide social behavior.

### 1.4 Encoding of anxiety-related information in the mPFC

Anxiety-related behaviors have evolved as adaptive responses to potential threats. These behaviors can enhance survival or become maladaptive depending on the intensity and context of the perceived threat. To appropriately respond to threat, animals must constantly assess their environment and internal state, balancing the need for vigilance with the costs of excessive avoidance. This balance is mediated by a distributed network of brain regions that detect, evaluate, and coordinate behavioral and physiological responses to stressors. This neural network allows for the flexible modulation of threat responses based on context and prior experience.[40] However, dysregulation within this network can lead to maladaptive anxiety, characterized by exaggerated threat perception and persistent avoidance.[40] Such maladaptive states are a hallmark of anxiety disorders and have become a major focus in both basic neuroscience and clinical research.

Within this threat-processing network, the mPFC plays a critical role in the regulation of anxiety by integrating cognitive, emotional, and physiological responses to stressors.[41,10,42,43] It exerts top-down control over subcortical regions such as the amygdala, which is heavily involved in threat processing.[10] Through its regulatory circuits, the mPFC can modulate the intensity and expression of anxiety-related behaviors.[10] Moreover, the mPFC is involved in the extinction of conditioned fear, further supporting its role in flexible, context-dependent regulation of anxiety and related states.[44,45] Through its extensive connections with both limbic and autonomic control centers, the mPFC serves as a hub for coordinating emotional state with physiological arousal, promoting flexible goal-directed behavior.[21-24] Disruptions of these mPFC-mediated processes can lead to maladaptive anxiety responses. When the mPFC is dysregulated (through hypoactivity), its ability to exert top-down control over brain regions like the amygdala is compromised.[10] Additionally, increases in mPFC VIP interneuron activity help generate prefrontal representations of open arm avoidance.[43] This can result in exaggerated threat perception, such as decreases in open arm time when mice are exposed to the elevated plus maze task. Evidence from lesion studies have shown that rodents with targeted lesions to the prelimbic or infralimbic subregions of the mPFC display heightened anxiety-like behaviors, such as increased avoidance in open field or elevated plus maze tests.[46] Complementary evidence comes from studies involving genetic mutations that affect mPFC function. Mice with mutations of genes involved in synapse formation and maintenance within the mPFC, like NRXN1 have been linked to heightened anxiety phenotypes.[47] Further support for mPFC's role in

anxiety regulation comes from optogenetic studies, which allow for cell-type specific manipulation of neural circuits.

Optogenetic activation of basolateral amygdala (BLA) neurons that project to the mPFC has been shown to increase anxiety-like behaviors, while optogenetic inhibition of BLA neurons that project to the mPFC reduce avoidance behaviors.[48,49] Additionally, optogenetic stimulation of vmPFC projections to the BMA reduce anxiety-like behaviors, while inhibition increases anxiety-like behaviors.[10,49] Furthermore, optogenetic modulation of mPFC projections to downstream regions such as the periaqueductal gray has revealed circuit-specific control over anxiety-related behaviors.[50] These findings highlight the causal role of mPFC activity in shaping anxiety-related behaviors and provide mechanistic insight into how specific neural pathways contribute to emotional regulation.

Additionally, dysregulation of the mPFC can profoundly impact autonomic balance and stress reactivity. Lesion studies provide evidence for this role of the mPFC in autonomic regulation. For example, rodents with lesions to the mPFC show elevated heart rate response during mental stress, indicating a loss of inhibitory control over physiological stress responses.[51] Furthermore, electrical stimulation of the infralimbic subregion of the mPFC results in decreased heart rate, but fails to do so when the NTS is inhibited using muscimol, suggesting the mPFC-NTS pathway contributes to mPFC-mediated parasympathetic activation.[52] Optogenetic studies further support the role of the mPFC in autonomic and anxiety regulation. Selective activation of vmPFC neurons projecting

to the BMA has been shown to reduce heart rate and attenuate anxiety-like behaviors, highlighting a direct inhibitory influence on autonomic output.[10] Therefore, the mPFC plays a crucial modulatory role in maintaining physiological homeostasis under stress, acting through distinct subregions and circuit-specific pathways to balance sympathetic and parasympathetic outflow.

## 1.5 References


1. Engelhardt, E. (2018). Cerebral localization of the mind and higher functions The beginnings. *Dementia & neuropsychologia*, *12*(3), 321-325.
2. Smith, C. U. M. (2013). Cardiocentric Neurophysiology: The Persistence of a Delusion. *Journal of the History of the Neurosciences*, *22*(1), 6–13.
3. Lang, P. J. (1994). The varieties of emotional experience: a meditation on James-Lange theory. *Psychological review*, *101*(2), 211.
4. Fehr, F. S., & Stern, J. A. (1970). Peripheral physiological variables and emotion: the James-Lange theory revisited. *Psychological Bulletin*, *74*(6), 411.
5. Cannon, W. B. (1927). The James-Lange theory of emotions: A critical examination and an alternative theory. *The American journal of psychology*, *39*(1/4), 106-124.
6. Schachter, S., & Singer, J. (1962). Cognitive, social, and physiological determinants of emotional state. *Psychological review*, *69*(5), 379.
7. Barrett, L. F. (2017). The theory of constructed emotion: an active inference account of interoception and categorization. *Social cognitive and affective neuroscience*, *12*(1), 1-23.
8. LeDoux, J. E., & Pine, D. S. (2016). Using neuroscience to help understand fear and anxiety: a two-system framework. *American journal of psychiatry*, *173*(11), 1083-1093.
9. Hsueh, B., Chen, R., Jo, Y., Tang, D., Raffiee, M., Kim, Y. S., ... & Deisseroth, K. (2023). Cardiogenic control of affective behavioural state. *Nature*, *615*(7951), 292-299.

10. Adhikari, A., Lerner, T. N., Finkelstein, J., Pak, S., Jennings, J. H., Davidson, T. J., ... & Deisseroth, K. (2015). Basomedial amygdala mediates top-down control of anxiety and fear. *Nature*, *527*(7577), 179-185.
11. Lagatta, D. C., Fassini, A., Terzian, A. L., Corrêa, F. M., & Resstel, L. B. (2023). The medial prefrontal cortex and the cardiac baroreflex activity: physiological and pathological implications. *Pflügers Archiv-European Journal of Physiology*, *475*(3), 291-307.
12. Cutsforth-Gregory, J. K., & Benarroch, E. E. (2017). Nucleus of the solitary tract, medullary reflexes, and clinical implications. *Neurology*, *88*(12), 1187-1196.
13. Ricardo, J. A., & Koh, E. T. (1978). Anatomical evidence of direct projections from the nucleus of the solitary tract to the hypothalamus, amygdala, and other forebrain structures in the rat. *Brain research*, *153*(1), 1-26.
14. Hoover, W. B., & Vertes, R. P. (2007). Anatomical analysis of afferent projections to the medial prefrontal cortex in the rat. *Brain Structure and Function*, *212*, 149-179.
15. Sun, Q., Li, X., Ren, M., Zhao, M., Zhong, Q., Ren, Y., ... & Luo, Q. (2019). A whole-brain map of long-range inputs to GABAergic interneurons in the mouse medial prefrontal cortex. *Nature neuroscience*, *22*(8), 1357-1370.
16. Ährlund-Richter, S., Xuan, Y., van Lunteren, J. A., Kim, H., Ortiz, C., Pollak Dorocic, I., ... & Carlén, M. (2019). A whole-brain atlas of monosynaptic input targeting four different cell types in the medial prefrontal cortex of the mouse. *Nature neuroscience*, *22*(4), 657-668.

17. Pollatos, O., & Schandry, R. (2004). Accuracy of heartbeat perception is reflected in the amplitude of the heartbeat-evoked brain potential. *Psychophysiology*, *41*(3), 476-482.
18. Azzalini, D., Buot, A., Palminteri, S., & Tallon-Baudry, C. (2021). Responses to heartbeats in ventromedial prefrontal cortex contribute to subjective preference-based decisions. *Journal of Neuroscience*, *41*(23), 5102-5114.
19. Park, H. D., Correia, S., Ducorps, A., & Tallon-Baudry, C. (2014). Spontaneous fluctuations in neural responses to heartbeats predict visual detection. *Nature neuroscience*, *17*(4), 612-618.
20. Sakaki, M., Yoo, H. J., Nga, L., Lee, T. H., Thayer, J. F., & Mather, M. (2016). Heart rate variability is associated with amygdala functional connectivity with MPFC across younger and older adults. *Neuroimage*, *139*, 44-52.
21. Hurley, K. M., Herbert, H., Moga, M. M., & Saper, C. B. (1991). Efferent projections of the infralimbic cortex of the rat. *Journal of Comparative Neurology*, *308*(2), 249-276.
22. Terreberry, R. R., & Neafsey, E. J. (1983). Rat medial frontal cortex: a visceral motor region with a direct projection to the solitary nucleus. *Brain research*, *278*(1-2), 245-249.
23. Van Der Kooy, D., McGinty, J. F., Koda, L. Y., Gerfen, C. R., & Bloom, F. E. (1982). Visceral cortex: a direct connection from prefrontal cortex to the solitary nucleus in rat. *Neuroscience letters*, *33*(2), 123-127.

24. Van der Kooy, D., Koda, L. Y., McGinty, J. F., Gerfen, C. R., & Bloom, F. E. (1984). The organization of projections from the cortes, amygdala, and hypothalamus to the nucleus of the solitary tract in rat. *Journal of Comparative Neurology*, *224*(1), 1-24.
25. Schaeuble, D., Packard, A. E., McKlveen, J. M., Morano, R., Fourman, S., Smith, B. L., ... & Myers, B. (2019). Prefrontal cortex regulates chronic stress-induced cardiovascular susceptibility. *Journal of the American Heart Association*, *8*(24), e014451.
26. Resstel, L. B. M., & Corrêa, F. M. D. A. (2005). Pressor and tachycardic responses evoked by microinjections of l-glutamate into the medial prefrontal cortex of unanaesthetized rats. *European Journal of Neuroscience*, *21*(9), 2513-2520.
27. Grossmann, T. (2013). The role of medial prefrontal cortex in early social cognition. *Frontiers in human neuroscience*, *7*, 340.
28. Ko, J. (2017). Neuroanatomical substrates of rodent social behavior: the medial prefrontal cortex and its projection patterns. *Frontiers in neural circuits*, *11*, 41.
29. Isoda, M. (2021). The role of the medial prefrontal cortex in moderating neural representations of self and other in primates. *Annual Review of Neuroscience*, *44*(1), 295-313.
30. Holsen, L. M., Dalton, K. M., Johnstone, T., & Davidson, R. J. (2008). Prefrontal social cognition network dysfunction underlying face encoding and social anxiety in fragile X syndrome. *Neuroimage*, *43*(3), 592-604.
31. Bicks, L. K., Koike, H., Akbarian, S., & Morishita, H. (2015). Prefrontal cortex and social cognition in mouse and man. *Frontiers in psychology*, *6*, 1805.

32. Osman, A., Mervosh, N. L., Strat, A. N., Euston, T. J., Zipursky, G., Pollak, R. M., ... & Kiraly, D. D. (2023). Acetate supplementation rescues social deficits and alters transcriptional regulation in prefrontal cortex of Shank3 deficient mice. *Brain, behavior, and immunity*, *114*, 311-324.
33. Selimbeyoglu, A., Kim, C. K., Inoue, M., Lee, S. Y., Hong, A. S., Kauvar, I., ... & Deisseroth, K. (2017). Modulation of prefrontal cortex excitation/inhibition balance rescues social behavior in CNTNAP2-deficient mice. *Science translational medicine*, *9*(401), eaah6733.
34. Yizhar, O., Fenno, L. E., Prigge, M., Schneider, F., Davidson, T. J., O'shea, D. J., ... & Deisseroth, K. (2011). Neocortical excitation/inhibition balance in information processing and social dysfunction. *Nature*, *477*(7363), 171-178.
35. Huang, W. C., Zucca, A., Levy, J., & Page, D. T. (2020). Social behavior is modulated by valence-encoding mPFC-amygdala sub-circuitry. *Cell reports*, *32*(2).
36. Franklin, T. B., Silva, B. A., Perova, Z., Marrone, L., Masferrer, M. E., Zhan, Y., ... & Gross, C. T. (2017). Prefrontal cortical control of a brainstem social behavior circuit. *Nature neuroscience*, *20*(2), 260-270.
37. Brumback, A. C., Ellwood, I. T., Kjaerby, C., Iafrati, J., Robinson, S., Lee, A. T., ... & Sohal, V. S. (2018). Identifying specific prefrontal neurons that contribute to autism-associated abnormalities in physiology and social behavior. *Molecular psychiatry*, *23*(10), 2078-2089.
38. Levy, D. R., Tamir, T., Kaufman, M., Parabucki, A., Weissbrod, A., Schneidman, E., & Yizhar, O. (2019). Dynamics of social representation in the mouse prefrontal cortex. *Nature neuroscience*, *22*(12), 2013-2022.

39. Frost, N. A., Haggart, A., & Sohal, V. S. (2021). Dynamic patterns of correlated activity in the prefrontal cortex encode information about social behavior. *PLoS biology*, *19*(5), e3001235.
40. Calhoon, G. G., & Tye, K. M. (2015). Resolving the neural circuits of anxiety. *Nature neuroscience*, *18*(10), 1394-1404.
41. Adhikari, A., Topiwala, M. A., & Gordon, J. A. (2010). Synchronized activity between the ventral hippocampus and the medial prefrontal cortex during anxiety. *Neuron*, *65*(2), 257-269.
42. Padilla-Coreano, N., Bolkan, S. S., Pierce, G. M., Blackman, D. R., Hardin, W. D., Garcia-Garcia, A. L., ... & Gordon, J. A. (2016). Direct ventral hippocampal-prefrontal input is required for anxiety-related neural activity and behavior. *Neuron*, *89*(4), 857-866.
43. Lee, A. T., Cunniff, M. M., See, J. Z., Wilke, S. A., Luongo, F. J., Ellwood, I. T., ... & Sohal, V. S. (2019). VIP interneurons contribute to avoidance behavior by regulating information flow across hippocampal-prefrontal networks. *Neuron*, *102*(6), 1223-1234.
44. Milad, M. R., & Quirk, G. J. (2002). Neurons in medial prefrontal cortex signal memory for fear extinction. *Nature*, *420*(6911), 70-74.
45. Quirk, G. J., Garcia, R., & González-Lima, F. (2006). Prefrontal mechanisms in extinction of conditioned fear. *Biological psychiatry*, *60*(4), 337-343.
46. Jinks, A. L., & McGregor, I. S. (1997). Modulation of anxiety-related behaviours following lesions of the prelimbic or infralimbic cortex in the rat. *Brain research*, *772*(1-2), 181-190.

47. Wu, D., Zhu, J., You, L., Wang, J., Zhang, S., Liu, Z., ... & Chi, X. (2023). NRXN1 depletion in the medial prefrontal cortex induces anxiety-like behaviors and abnormal social phenotypes along with impaired neurite outgrowth in rat. *Journal of neurodevelopmental disorders*, *15*(1), 6.
48. Felix-Ortiz, A. C., Burgos-Robles, A., Bhagat, N. D., Leppla, C. A., & Tye, K. M. (2016). Bidirectional modulation of anxiety-related and social behaviors by amygdala projections to the medial prefrontal cortex. *Neuroscience*, *321*, 197-209.
49. Hare, B. D., & Duman, R. S. (2020). Prefrontal cortex circuits in depression and anxiety: contribution of discrete neuronal populations and target regions. *Molecular psychiatry*, *25*(11), 2742-2758.
50. Qian, J., Wu, W., Qiu, L., Liu, X., Luo, Y., Chen, F., ... & Qi, R. (2025). Medial prefrontal cortex-periaqueductal gray circuit overcomes anxiety-like behavior in male mice following adversity. *Journal of Affective Disorders*, *372*, 149-159.
51. Chen, X., Xu, L., & Li, Z. (2022). Autonomic neural circuit and intervention for comorbidity anxiety and cardiovascular disease. *Frontiers in Physiology*, *13*, 852891.
52. Sevoz-Couche, C., Comet, M. A., Bernard, J. F., Hamon, M., & Laguzzi, R. (2006). Cardiac baroreflex facilitation evoked by hypothalamus and prefrontal cortex stimulation: role of the nucleus tractus solitarius 5-HT2A receptors. *American Journal of Physiology-Regulatory, Integrative and Comparative Physiology*, *291*(4), R1007-R1015.

## Chapter 2 – Identification of neurocardiac networks in the mPFC

### 2.1 Introduction

The interaction between the brain and the heart has captivated curiosity since ancient times, with early civilizations debating whether cognition and emotion arose from the heart or the brain.[1] Ancient Egyptians viewed the heart as the seat of the soul, while Greek philosophers like Aristotle believed it was the source of thought and emotion.[2,3] It was not until later, with Hippocrates and Galen, that the brain began to be recognized as central to mental function.[3] Today, this old question has evolved into a scientific inquiry that sought to determine how neural and cardiac systems dynamically interact to shape behavior and physiological states, particularly in conditions of heightened arousal such as social interactions and anxiety. The current state of the field has demonstrated that contextual cues (such as social or anxiety-related cues) are integrated in the brain, then the brain transmits arousal signals to the heart (primarily via the spinal cord and adrenal gland) through the release of catecholamines such as epinephrine and norepinephrine. These modulators trigger a physiological state of arousal, leading to rapid increases in heart rate and changes in HRV, which are hallmarks of heightened sympathetic activation. In turn, these cardiac changes are relayed back to the brain, which involves multiple afferent pathways, including the vagus nerve, spinal cord, and circulating factors in the bloodstream. Ultimately, these incoming cardiac signals are integrated by the brain, influencing neural computations that guide decision-making based on the internal state and external context (**Figure 2.1A)**.

The development of modern cardiac monitoring technologies such as ECG have significantly advanced our understanding of cardiac function in humans exposed to different behavioral contexts. However, the challenge of accessing the human brain pose a limitation for recording neural activity with single-cell resolution during natural behaviors. This limitation has led researchers to turn to animal models, particularly mice, to study brain function with greater spatial and temporal precision. While mice provide unparalleled access to the brain at single-cell resolution, recording cardiac activity in freely moving mice presents its own set of technical challenges. The small size and high heart rate of mice require highly sensitive equipment, and their rapid movements produce signal artifacts that can distort ECG signals. To address this limitation, we developed a method for simultaneously performing microendoscopic calcium imaging and ECG recordings in freely moving mice. This integrated approach allows us to uncover how brain regions participate in the central integration of cardiac function and characterize groups of neurons that encode cardiac signals such as heart rate or HRV.

For instance, neurons in the mPFC have been shown to modulate their activity in phase with cardiac rhythms.[4] Using techniques such as cardiac optogenetics, researchers have identified neurons in the mPFC whose activity increase (as shown by increases in cFos immunoreactivity) when delivering tachycardic stimuli to the heart.[5] Additionally, theta-frequency (7 Hz) stimulation of mPFC neurons projecting to the thalamus produces bradycardia (i.e. decreases in heart rate).[6] Furthermore, stronger functional coupling between the mPFC and the amygdala is associated with higher HRV, whereas

weaker functional coupling between both regions is associated with reduced HRV.[7] However, our understanding of how heart-related signals are mapped at the single-cell level within the mPFC remains limited, highlighting the need for simultaneous high-resolution neural and heart rate recordings in freely behaving animals. Given the complex cellular heterogeneity within the mPFC and the role of this region in monitoring and modulating heart rate, one might expect to find neural subpopulations that are correlated, anti-correlated, or uncorrelated with heart rate or HRV. Interestingly, with our technical approach to simultaneously record calcium signals and heart rate in the same mouse, we do find mPFC neurons with activity that is positively correlated or negatively correlated with heart rate (which we termed as “neurocardiac networks”). We were able to identify an additional subpopulation of mPFC neurons with patterns of activity that are uncorrelated with heart rate. Surprisingly, our technical approach shows that the activity of mPFC neurons at the single-cell level is poorly correlated to HRV, suggesting that this influence may arise from broader network dynamics rather than from individual neurons, or that the mPFC primarily modulates HRV without strongly integrating this information.

## 2.2 Materials and Methods

### Animal Subjects

All animal care procedures and experiments were conducted in accordance with the National Institutes of Health guidelines and approved by the Administrative Panels on Laboratory Animal Care at the University of California, San Francisco. Mice were housed in a temperature-controlled environment (22–24 °C) with ad libitum access to

food and water. Mice were reared in normal lighting conditions (12-h light/dark cycle). Male C57BL/6J mice (10-12 weeks old at the time of the microendoscopic surgery and 14-16 weeks at the time of the ECG surgery) were used.

**Surgical Procedures**

All animals used for experiments underwent a two-stage surgical protocol: one for viral delivery/GRIN lens implantation and another for implantation of ECG wires. During both procedures, mice were anesthetized with isoflurane delivered in 95% oxygen at a flow rate of 0.9 L/min. For viral delivery/GRIN lens implantation, animals were placed in a stereotaxic apparatus (David Kopf Instruments) using head bars for head fixation. Subcutaneous injections of Ethiqa XR (3.25 mg/kg) and meloxicam (2 mg/kg) were administered at the onset of surgery for analgesia. Body temperature was maintained with a heating pad throughout the procedure. The local anesthetic lidocaine was injected in the incision site and a midline incision was made along the scalp to expose the skull, which was aligned using bregma and lambda. Following surgery, animals were kept on a heating pad for recovery until fully ambulatory. A second dose of meloxicam was administered the day after surgery. For implantation of ECG wires, animals were anesthetized using an anesthesia face mask (Kent Scientific) and placed on a heating pad to maintain body temperature. Subcutaneous injections of Ethiqa XR (3.25 mg/kg) and meloxicam (2 mg/kg) were administered at the onset of surgery for analgesia. The local anesthetic lidocaine was injected in the incision site and a midline incision was made along the chest to expose the chest muscles. Following surgery,

animals were kept on a heating pad for recovery until fully ambulatory. A second dose of meloxicam and 1 mL of sterile saline was administered the day after surgery.

Viral injections and GRIN lens implantation were carried out in mice aged 10-12 weeks old. A 0.6 mm craniotomy was made above the right mPFC at coordinates +1.7 mm anterior-posterior (AP) and +0.3 mm medial-lateral (ML) relative to bregma using a dental drill. The viral construct AAV9-hSyn-jGCaMP7f-WPRE (AddGene) was diluted 1:3 in sterile saline prior to injection. Using a 35-gauge syringe (World Precision Instruments) connected to a UMP3 UltraMicroPump, 150 nL of virus was infused at four depths (-2.00 mm, -2.25 mm, -2.50 mm, -2.75 mm dorsal-ventral [DV]) at a flow rate of 150 nL/min. The syringe remained in place for five minutes following each injection to prevent backflow. After five minutes, the syringe was slowly removed from the brain and a GRIN lens implantation was performed. A 0.5 mm x 4.0 mm GRIN lens (Inscopix) was lowered through the 0.6 mm craniotomy to a depth of -2.3 mm and secured to the skull using Metabond (Parkell). Postoperatively, mice were singly housed and given four weeks to recover before performing the ECG surgery.

ECG surgeries were carried out in mice aged 14-16 weeks old that were implanted with GRIN lenses. Four perfluoroalkoxy-coated stainless steel wires (791000, A-M Systems) soldered to a 8-pin mouse headmount (8415-SM, Pinnacle Technology) were tunneled through the back of the mouse until they reach the chest. The wires were secured on the chest muscles with non-absorbable sutures while making sure the recording sites of each wire did not make contact. From the four stainless steel wires, two pick up ECG

signals, one was the ground, and one serves as an anchor and provides additional support to diminish movement artifacts. After suturing the wires to the chest muscles, the incision was closed with sutures. Then, the animals were placed in the stereotaxic apparatus and the headmount was secured to the skull with metabond and dental acrylic (Ortho-Jet, Patterson Dental). Postoperatively, mice were singly housed and given at least four days to recover before performing experiments.

After experiments, mice were intracardially perfused with 4% paraformaldehyde (PFA) to verify GRIN lens placement and the injection site of the viral construct in the mPFC.

**Behavioral Tasks**

Mice underwent a habituation period to acclimate them to the head-mounted microscope over the course of 2 weeks. Additionally, they were habituated to experimenter handling for four consecutive days, with each session lasting 10 minutes. On testing days, mice were transported to the behavioral room 1 hour prior to the start of the experiment to allow for acclimation. Before the beginning of the experiment, the animals were plugged to the head-mounted microscope and the ECG pre-amplifier for 20 minutes and left undisturbed to allow recovery from the brief stress associated with handling and equipment attachment.

*Resting period recordings to identify neurocardiac networks*

To examine resting-state activity across behavioral and pharmacological conditions, mice underwent two experimental sessions on separate days. Each session included

periods of behavioral engagement interleaved with designated rest epochs, during which animals were left undisturbed in their home cage under the same recording conditions.

On Day 1, mice underwent a sequence of behavioral and resting periods beginning with a 15-minute baseline rest recording, followed by 5 minutes of novel object exploration (NOE). This was followed by a 5-minute post-NOE rest period, then 10 minutes of social interaction with a juvenile conspecific, and a subsequent 5-minute rest. Mice then engaged in a 20-minute social interaction with a CD1 aggressor, followed by another 5-minute rest. The session concluded with a 15-minute pharmacology baseline rest and a 45-minute period of pharmacological stimulation. On Day 2, the experimental structure was similar: mice began with a 15-minute baseline rest, followed by 15 minutes in the elevated plus maze (EPM), a 5-minute post-EPM rest, a second 15-minute pharmacology baseline rest, and finally, 45 minutes of pharmacological stimulation. Resting periods used for subsequent analyses included the baseline recording, post-behavioral rest epochs, and pharmacology baseline segments. Specifically, rest epochs on Day 1 included the baseline (15 minutes), post-NOE rest (5 minutes), post-social interaction with a juvenile rest (5 minutes), post-social interaction with an aggressor rest (5 minutes), and pharmacology baseline (15 minutes). On Day 2, rest periods included the baseline (15 minutes), post-EPM rest (5 minutes), and pharmacology baseline (15 minutes). These resting periods were selected to minimize neural signatures associated with behavioral conditions or pharmacological manipulation, thereby enabling the identification of neurocardiac networks.

**Data Acquisition and Processing**

Calcium signals were imaged at 20 Hz with 4x downsampling using a head-mounted 1-photon microendoscope (nVoke2, Inscopix Inc.). Calcium videos were preprocessed using Inscopix Data Processing Software (IDPS), including spatial band-pass filtering with cutoffs set to 0.008 pixel-1 (low) and 0.500 pixel-1 (high), followed by motion correction. Preprocessed calcium videos were exported from IDPS as NWB files, converted to HDF5 format using HDFView, and then imported into MATLAB for cell segmentation. Putative cellular ROIs were identified and DF/F signals were extracted using EXTRACT.[8] For each calcium movie, putative neurons were manually curated to remove ROIs with low signal-to-noise ratio or overlapping boundaries. Cell sorting was done with the assistance of the signalSorter GUI from the open-source calcium imaging analysis package (CIAPKG).[9] Calcium signal (DF/F) from each neuron was averaged in 1-second segments.

ECG signals were acquired at 10 KHz using a head-mounted 4-channel mouse preamplifier (8406-SE4, Pinnacle Technology) connected to a 9-pin commutator (8401-HS, Pinnacle Technology) from the data acquisition system. Signals were filtered with a high-pass cutoff of 10 Hz and a low-pass cutoff between 200-300 Hz. Preprocessed ECG recordings were exported from Sirenia software as EDF files and subsequently imported into MATLAB for further analysis. ECG data were converted from frames to seconds. Segments with motion artifacts were manually curated or excluded if the signal was significantly distorted. Custom MATLAB code was used to detect R-peaks, corresponding to individual heartbeats, from the ECG signal. Heart rate was calculated

as the sum of R-peaks in 1-second segments. HRV was calculated as the bin-to-bin deviations in heart rate (using standard deviation calculations). Specifically, HRV was computed as the difference in heart rate between consecutive 1-second bins. Behavioral videos were recorded at 25 frames per second using Sirenia software. A TTL cable connecting the data acquisition system with the Inscopix DAQ box was used to temporally align the behavioral videos with ECG signals and calcium imaging data.

**Data Analysis**

All analyses of calcium activity and ECG signal were performed using code written in MATLAB.

*Analysis to identify neurocardiac networks*

Custom scripts were written in MATLAB to determine if calcium activity (DF/F in 1-second bins) of individual neurons was significantly associated with a cardiac signal (i.e., heart rate or HRV, also binned in 1-second segments). To do this, we identified frames corresponding to resting periods across sessions. For each neuron, we computed the Pearson correlation between its calcium activity and the heart rate or HRV of the animal during those periods. This observed correlation was then compared to a null distribution generated by circularly shuffling the heart rate or HRV signal 1,000 times.

Neurons were considered significantly positively correlated (i.e., +HR or +HRV encoders) if their true correlation exceeded the 95th percentile of the shuffled

distribution, and significantly negatively correlated (i.e., -HR or -HRV encoders) if their correlation fell below the 5th percentile. Neurons with correlation values between the 5th and 95th percentiles were classified as HR or HRV non-encoders.

*Mean activity of neurocardiac networks during resting periods*

To calculate each neuron's (i.e., +HR encoders, +HRV encoders, -HR encoders, -HRV encoders, HR non encoders, and HRV non-encoders) mean activity during resting periods, we first averaged the DF/F signal into 1-second segments. We then computed the mean activity as a z-score, normalized relative to the shuffled DF/F signal.

*Shuffle-based analysis of heart rate correlations*

To assess whether correlations between neural activity and heart rate were driven by structured temporal relationships, we implemented a shuffled-based analysis across multiple timescales. Specifically, we calculated the Pearson correlation coefficient between calcium activity (DF/F in 1-second bins) of each neural population (i.e., +HR encoders, -HR encoders, and HR non-encoders) and the corresponding heart rate signal (heartbeats in 1-second bins) during resting periods. To generate a null distribution, we then temporally shuffled the heart rate signal within non-overlapping segments of varying lengths (5, 10, 20, 30, 60, 120, 180, 240, and 300 seconds). Within each segment, heart rate values were randomly permuted to preserve local heart rate statistics while disrupting temporal alignment. This procedure was repeated across all timescales, and for each shuffled heart rate signal, we recalculated the neuron-by-heart

rate correlations. We then computed the mean correlation across neurons from each neural population for both the original and shuffled heart rate signals.

## 2.3 Results

Mice were injected with virus to drive neuron-specific expression of a calcium indicator under the regulation of the synapsin promoter (i.e., syn-jCaMP7f) in neurons within the mPFC (**Figure 2.1B**). After waiting approximately 4 weeks, mice underwent a second surgery to implant electrodes for ECG recordings (**Figure 2.1C**). After waiting 4 days for mice to recover from this second procedure, we performed simultaneous single-cell calcium imaging and ECG recordings (**Figure 2.1D-E**) while freely moving mice underwent a series of behavioral tests over two days (**Figure 2.1F**). On the first day, mice were recorded during a 15 minute of baseline period, followed by (NOE) (5 min), a rest period (5 min), interaction with a juvenile mouse (10 min), another rest period (5 min), interaction with a CD1 aggressor (20 min), a final rest period (20 min), and during the response to an injection of isoproterenol (iso) (45 min). On the second day, mice were recorded during a 15 minute baseline period, followed by elevated plus maze exploration (15 minutes), a rest period (20 min), and during another response to iso injection (45 min). Some mice (n = 3) were injected with saline instead of iso as a control.

*Prefrontal neurocardiac networks*

As mentioned before, mice underwent four rest periods (for a total of 45 mins) that enable us to capture the heart rate dynamics in baseline periods before behavior and

following behavior. We used these baseline periods to identify mPFC neurons with activity that is coupled to heart rate. To do this, we averaged the calcium activity (i.e., DF/F) of individual neurons and the heart rate/HRV over 1 second bins and then computed the Pearson correlation values between each signal (calcium activity and either heart rate or HRV), enabling the identification of neurons that are significantly positively correlated, negatively correlated (anticorrelated), or uncorrelated with heart rate/HRV (**Figure 2.2A**). In all mice (n = 8), we identified the mPFC neurons that positively or negatively encode heart rate above chance (i.e., p-value associated with the Pearson's correlated was < 0.05; **Figure 2.2B, left**) as well as mPFC neurons with non-significant correlations (i.e., p values > 0.05; **Figure 2.2B, right**). This yields three distinct populations of neurons: positive (+) HR encoders, negative (-) HR encoders, and HR non-encoders. We quantified the proportion of each neural population and found that +HR encoders comprised 19% of mPFC neurons, -HR encoders 13%, and HR non-encoders made up the remaining 68% (**Figure 2.3A, left**). Notably, the fractions of +HR or -HR encoders are both much higher than the fraction expected by chance (~5%). When comparing +HR encoders to the HR non-encoders which have positive (but non-significant) Pearson correlation values, or -HR encoders to HR non-encoders with negative (but non-significant) Pearson correlation values, we confirmed that as expected, the magnitude of correlations was significantly larger for +HR or -HR encoders compared to HR non-encoders (**Figure 2.2C**).

After identifying the HR encoders, we computed the mean heart rate and the mean calcium activity (for each neuron) in each baseline period. The heart rate and +HR

encoders follow parallel trajectories, whereas the -HR encoders follow an inverted trajectory, supporting the interpretation that both populations track heart rate dynamics in real-time (**Figure 2.2D**). As expected, there was no such relationship observed for the HR non-encoders (**Figure 2.5A**). We observed the same findings when we analyzed data from a second day of experiments, using baseline periods before and after EPM exploration (**Figure 2.4A-D, Figure 2.5B**).

This finding raises a question: how rapidly (over what timescale) do these neural populations track changes in the heart rate? To address this, we first computed the autocorrelation of the baseline heart rate signal across a range of time lags, spanning form 1 second to 5 minutes. By correlating the heart rate signal with time-shifted versions of itself at short (1-10 sec), medium (10-60 sec), and long (60-300 sec) intervals, we assessed the intrinsic temporal structure of the heart rate dynamics. We observed a modest decline in autocorrelation over short timescales, and more pronounced decreases at medium and long timescales (the autocorrelation fell to ~60% of its peak value when shuffled on timescales ~10 sec, was ~30% of its peak when shuffled on timescales ~60 sec, and was near 0 when shuffled on timescales > 120 sec; **Figure 2.2E, upper panel**). These results suggest that the heart rate (averaged over 1 second bins) fluctuates on both short (< 10 sec) and medium (10-100 sec) timescales, and is largely uncorrelated on timescales > 120sec. After characterizing these intrinsic timescales for heart rate fluctuations, we examined how HR encoders align with these dynamics and the timescales over which these populations encode heart rate. To do this, we systematically disrupted the temporal structure of the heart rate signal by

shuffling it within non-overlapping windows of increasing duration (ranging from 5 to 300 sec), and then computed the correlation between each HR encoder's baseline activity and the shuffled heart rate signal. A sharp drop or increase in correlation when heart rate is shuffled at shorter timescales would suggest that +HR and -HR encoders track heart rate fluctuations over brief windows, respectively. The opposite is expected if significant changes in correlation occur at longer timescales. We found that shuffling at shorter timescales (5-10 sec) had minimal effect on the correlation for both +HR and -HR encoders (correlations were reduced by <10%), whereas shuffling at medium and longer timescales (10-60 sec and 60-300 sec, respectively) caused the magnitudes of correlation to decrease by about 30% or 50% respectively for both +HR and -HR encoders (**Figure 2.2E, middle panel and lower panel**). Shuffling at the timescales previously described did not lead to significant changes in the correlation values of HR non-encoders (**Figure 2.5C**). These results indicate that +HR and -HR encoders encode information over similar timescales, and that whereas HR changes on both fast (<10 sec) and slow (10-100 sec) timescales, HR encoders are more strongly influenced by slow dynamics on timescales of 10-100 sec of seconds.

Having established that specific mPFC neurons encode heart rate dynamics, we next asked whether a subset of these neurons also exhibit activity patterns coupled to HRV, a distinct but related cardiac signal. To address this, we first defined HRV in mice as the bin-to-bin deviations in heart rate (using 1-second bins). Specifically, HRV was computed as the difference in heart rate between consecutive 1-second bins. We chose 1-second bins to account for the temporal resolution mismatch between heart rate and

calcium signals, as calcium transients typically evolve over ~1 sec. To align the timescales and ensure meaningful comparisons, both heart rate and calcium activity data were binned at 1-second intervals. We then computed the Pearson correlation between HRV and the average calcium activity of each neuron. We found mPFC neurons that positively or negatively encode HRV above chance (i.e., were significantly correlated using a p-value threshold of 0.05; **Figure 2.2F, left**). However, both the number of such neurons, and the associated correlation values were much lower compared to what we observed for HR encoders. We also identified mPFC neurons with non-significant correlations (**Figure 2.2F, right**), yielding three distinct neural populations: positive (+) HRV encoders, negative (-) HRV encoders, and HRV non-encoders. We quantified the proportion of each neural population and found that +HRV encoders comprised 5% of mPFC neurons, -HRV encoders 6%, and HR non-encoders made up the remaining 89% (**Figure 2.3A, right**). Thus, the numbers of +HRV and -HRV encoders is not meaningfully different from the levels expected by chance. This suggests that mPFC neurons only weakly encode HRV. When comparing +HRV encoders to HRV non-encoders with positive (but non-significant) Pearson correlation values, or -HRV encoders to HRV non-encoders with negative (but non-significant) Pearson correlation values, we confirmed that the magnitude of correlations was significantly greater for both +HRV or -HRV encoders compared to HRV non-encoders. However, the effect size was smaller than that observed for HR encoders (**Figure 2.2C, Figure 2.2G**). Additionally, we computed the mean HRV and mean calcium activity (for each neuron) in each baseline period. Notably, +HRV encoders followed the same trajectory as HRV signal, and -HRV encoders followed the opposite trajectory, but to a

lesser extent than the corresponding relationship between HR encoders and heart rate, supporting the interpretation that these neurons weakly track HRV dynamics in real-time (**Figure 2.2D, Figure 2.2H**). As expected, the HRV signal did not follow the trajectory of the HRV non-encoders (**Figure 2.6A**). We consistently observed the same findings on the second day of experiments, using baseline periods before and after EPM exploration (**Figure 2.4E-H, Figure 2.6B**). Together, these findings suggest that while a small subset of mPFC neurons may weakly encode HRV, this encoding is much less consistent than the encoding of heart rate.

## 2.4 Discussion

In this study, we developed and applied a method for simultaneous microendoscopic calcium imaging and ECG recordings in freely moving mice to uncover how neurons in the mPFC track heart rate and HRV in resting conditions. We identified three distinct subpopulations of mPFC neurons based on their coupling to heart rate: positively correlated ("+HR encoders"), negatively correlated ("-HR encoders"), and non-correlated ("HR non-encoders"). The +HR encoders and -HR encoders, which we collectively refer to as "neurocardiac networks", consistently tracked real-time HR dynamics across resting periods, with +HR and -HR encoders mirroring or opposing the trajectory of the heart rate signal, respectively. Surprisingly, the encoding of HRV was far less robust: although a small fraction of neurons was significantly correlated with HRV, the number of correlated neurons and correlation values were both much lower than for heart rate. Furthermore, the fraction of significantly correlated neurons was not markedly different from the chance level. This contrast between encoding of HR vs. HRV underscores that

the correlations we found with HR are biologically and statistically meaningful. Our temporal analyses (shuffling) also revealed that neurocardiac networks in the mPFC are mainly sensitive to changes in heart rate occurring over medium-to-long timescales (10-100 sec), supporting their role in encoding sustained cardiac states rather than transient, moment-to-moment fluctuations occurring on fast timescales (<10 sec). Together, these findings demonstrate that large subsets of mPFC neurons participate in the dynamic representation of internal cardiac states, preferentially tracking sustained changes in heart rate rather than HRV in real time.

Previous studies have established the mPFC as a hub for integrating autonomic signals, showing its involvement in modulating cardiovascular function. For instance, optogenetic stimulation of mPFC projections to the amygdala has been shown to induce bradycardia, and heightened mPFC-amygdala coupling has been associated with increased HRV (a marker of parasympathetic tone).[7,10] While these studies demonstrate a causal influence of mPFC activity on cardiovascular output, our results extend this body of work by revealing that cardiac signals are also represented within the mPFC at the single-neuron level. Furthermore, prior human studies have implicated prefrontal areas in heartbeat perception, but the spatial and temporal resolution of these methods have precluded insights into single-cell dynamics.[11,12] Our work fills this gap by showing that specific neurons in the mPFC reliably track heart rate across time, suggesting a local representation of internal physiological states that may contribute to interoceptive processes.

While our integrated imaging-ECG approach offers high spatiotemporal resolution, several limitations must be acknowledged. First calcium imaging has intrinsic limitations compared to electrophysiology that may have impacted our results. Calcium indicators have relatively slow kinetics, which can obscure fast or transient neuronal activity that might be better captured with electrical recordings. Second, our method captures correlations rather than causality; thus, while we can identify neurons whose activity co-varies with heart rate, we cannot determine whether these neurons actively regulate heart rate, receive cardiac feedback, or track a distinct internal variable which is itself correlated with heart rate (or some combination of these). Third, we computed heart rate and HRV in 1-second bins, which may have reduced our ability to detect finer-scale relationships. Additionally, we calculated neuron-heart rate correlations using rest periods in order to minimize potential confounds related to ongoing behavior. However, less overly-obvious behavioral variables (residual odors, replay events, stress, grooming, etc.) could still influence the heart rate and neural activity during these periods, potentially contributing to some of the observed correlations. Lastly, the relatively small proportion of HRV-encoding neurons may partly reflect technical limitations related to the way we defined and calculated HRV – it is possible that other metrics for heart rate variability may have led to different results.

Our findings have important implications for understanding how the brain represents internal bodily states and how these representations may shape behavior. The ability of mPFC neurons to encode sustained changes in heart rate states suggests that interoceptive information is not only broadcast to higher-order regions but is also locally

integrated by individual neurons. This supports emerging theories that link interoceptive coding to affective regulation, decision-making, and the evaluation of risk and reward (domains which the mPFC plays a central role). Notably our data highlight a preferential representation of tonic cardiac states (i.e., sustained heart rate) over phasic variability (i.e., HRV), suggesting that the mPFC may be more attuned to persistent changes in arousal or homeostasis rather than rapid beat-to-beat (or second-to-second) fluctuations. This distinction could be relevant to understanding how dysregulated brain-heart communication contributes to anxiety disorders, which are characterized by persistent hyperarousal and altered autonomic control. If activity within neurocardiac networks is altered in these states, it could impair the brain's ability to monitor and adapt to physiological changes, potentially exacerbating emotional reactivity or producing faulty behavioral regulation.

Several promising avenues for future research emerge from this work. First, causal manipulation of HR encoders using optogenetics or chemogenetics could clarify whether these populations directly influence cardiac output or are primarily involved in sensory monitoring. For instance, activating +HR encoders could hypothetically increase heart rate if they exert excitatory control over autonomic output pathways, whereas silencing -HR encoders might attenuate heart rate suppression. Alternatively, if manipulations do not affect heart rate, this would support a predominantly sensory or monitoring role. Second, mapping neurocardiac networks across other brain regions involved in interoception (e.g., insula, hypothalamus) could reveal whether similar encoding strategies exist elsewhere or are unique to the mPFC. Third, future studies

should examine how these networks change under stress or pathological conditions such as chronic anxiety, post-traumatic stress disorder, or depression, where both heart rate and HRV are dysregulated. In chronic stress models, for example, one might expect diminished sensitivity of neurocardiac networks to heart rate changes, reflecting reduced interoceptive precision, or even a shift in the balance between +HR and -HR encoders that could bias emotional and behavioral responses toward hyperarousal or impaired autonomic recovery. Finally, as we will explore in later chapters, integrating behaviorally contingent analysis (e.g. during approach-avoidance tasks) with neural-cardiac coupling metrics could reveal ways in which internal state representations interact with action selection. In sum, this work lays the groundwork for a more detailed understanding of brain-body integration and how neural circuits dynamically represent physiological states to guide adaptive behavior.

## 2.5 Figures

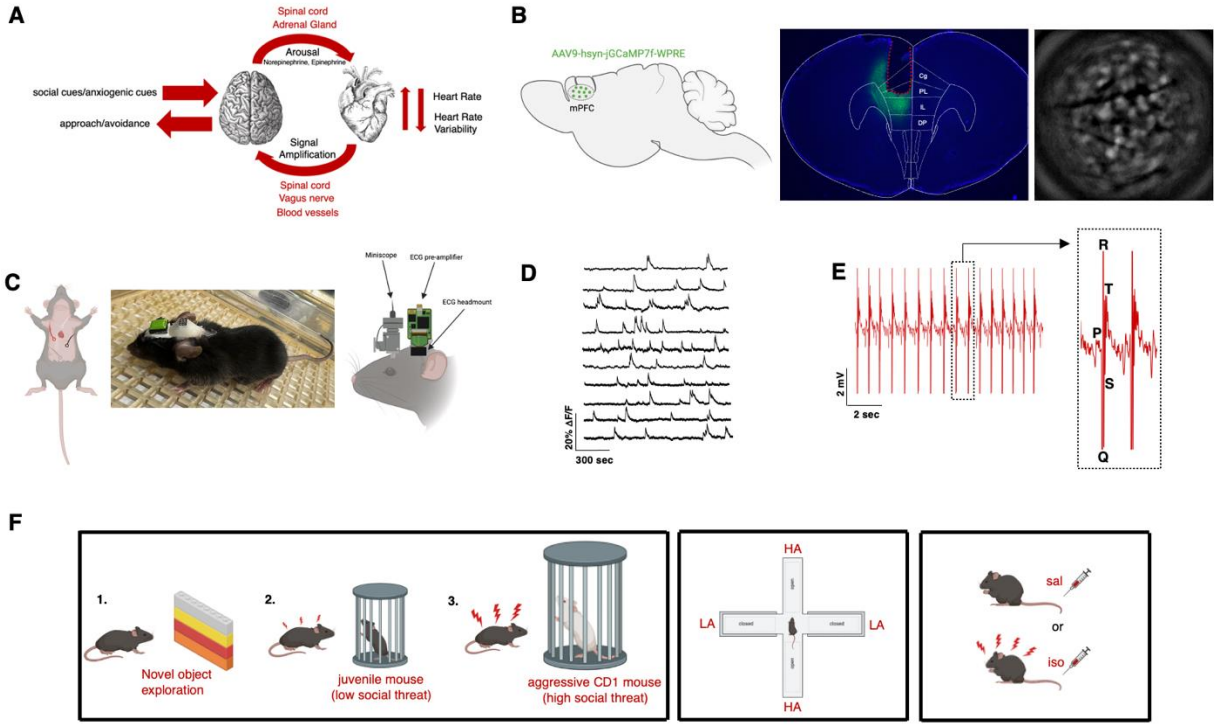


**Figure 2.1. Theoretical and experimental design to study neurocardiac networks during approach-avoidance behaviors**. (A) Theoretical diagram illustrating the bidirectional communication between the brain and the heart during behavior. (B) *Left*, schematic of the viral construct used to express GCaMP7f in the mPFC. *Middle*, Representative image showing GCaMP7f expression in the mPFC (green) and GRIN lens placement (scale bar, 1mm). *Right*, Field of view from a representative calcium imaging session. (C) *Left*, Schematic showing the placement of ECG wires implanted in the mouse. *Middle*, Photograph of a mouse implanted with a GRIN lens for calcium imaging and an ECG headmount. *Right*, Schematic of the miniscope, and the ECG preamplifier connected to the ECG headmount. (D) Representative DF/F calcium transients from individual neurons. (E) *Left*, Representative ECG trace. *Right*, Magnified view of individual heartbeats showing components of the cardiac cycle, including the P-wave, QRS complex, T-wave, S-T segment. (F) Behavioral paradigms used in the study. (HA: high anxiety, LA: low anxiety, sal: saline, iso: isoproterenol).

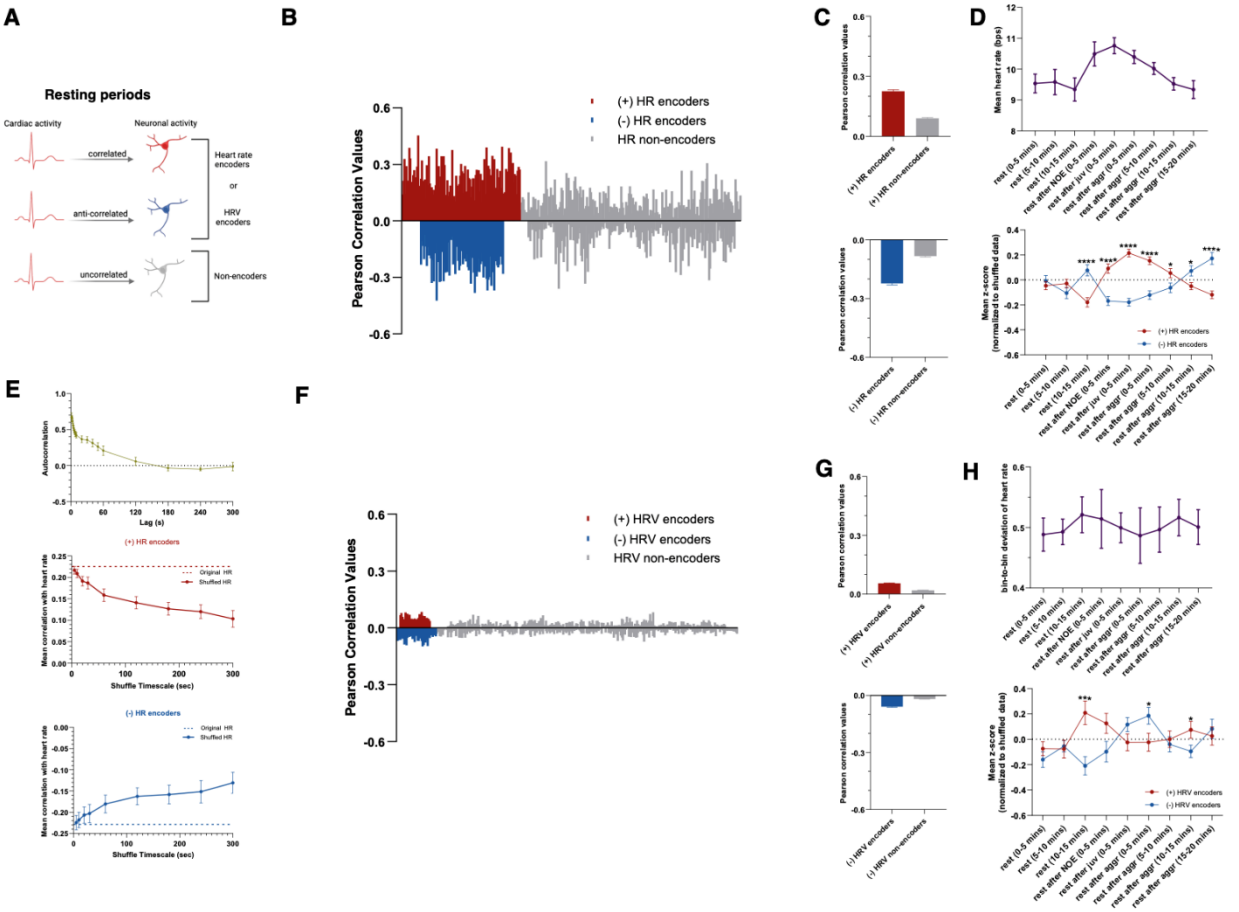


**Figure 2.2. Identification of neurocardiac networks in the mPFC.** (A) Schematic illustrating how neural activity is categorized based on its relationship to cardiac activity (e.g., heart rate or HRV). Neurons whose calcium activity is significantly positively correlated (red) or negatively correlated (blue) with cardiac signals are classified as heart rate or HRV encoders. Neurons whose activity does not significantly correlate with cardiac signals (gray) are classified as non-encoders. (B) Distribution showing the Pearson correlation values between calcium activity of individual neurons and heart rate during resting periods. Neurons with significantly positive correlations were classified as +HR encoders, and those with significantly negative correlations were classified as -HR encoders. Neurons whose correlation values did not exceed the 95th or fall below the 5th percentile of a shuffled null distribution were classified as HR non-encoders. (C) Bar graphs displaying mean Pearson correlation values between calcium activity and heart rate for each neural population. *Top*, Comparison between +HR encoders and HR non-encoders with positive correlation values. *Bottom*, Comparison between -HR encoders and HR non-encoders with negative correlation values. (D) *Top*, Mean heart rate across resting periods before behaviors and during resting periods following NOE, social interactions with a juvenile (juv), and exposure to an aggressor (aggr). Heart rate increased during resting periods following all behaviors and gradually returned toward baseline levels. *Bottom*, Mean z-scored activity of +HR encoders and -HR encoders across the same resting periods as (*Top*). (E) *Top*, Autocorrelation of heart rate across time lags during a resting period. *Middle*, Mean correlation of +HR encoders with heart rate across increasing temporal shuffling windows. Dashed red line indicates the correlation with unshuffled heart rate.*Bottom*, Same as middle, but for -HR encoders. (Figure caption continued on the next page)

(Figure caption continued from the previous page) Dashed blue line indicates original correlation with unshuffled heart rate (F) Distribution showing the Pearson correlation values between calcium activity of individualneurons and HRV during resting periods. Neurons with significantly positive correlations were classified as +HRV encoders, and those with significantly negative correlations were classified as -HRV encoders. Neurons whose correlation values did not exceed the 95th or fall below the 5th percentile of a shuffled null distribution were classified as HRV non-encoders. (G) Bar graphs displaying mean Pearson correlation values between calcium activity and heart rate for each neural population. *Top*, Comparison between +HRV encoders and HRV non-encoders with positive correlation values. *Bottom*, Comparison between -HRV encoders and HRV non-encoders with negative correlation values. (H) *Top*, Mean HRV across resting periods before behaviors and during resting periods following NOE, social interactions with a juvenile (juv), and exposure to an aggressor (aggr). HRV shows moderate fluctuations during resting periods without significant changes. *Bottom*, Mean z-scored activity of +HRV encoders and -HRV encoders across the same resting periods as (*Top*). Data are shown as mean ± SEM. *$p < 0.05$, ***$p < 0.001$, ****$p < 0.0001$, ($n = 8$ mice, 644 neurons).

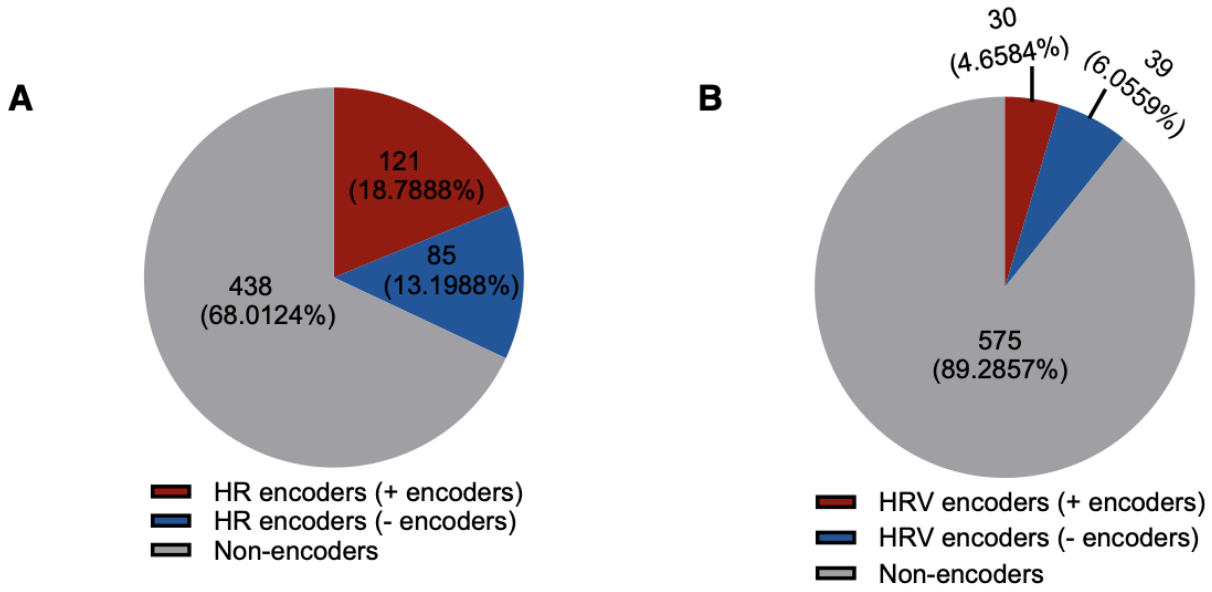


**Figure 2.3. Proportion of HR encoders and HRV encoders in the mPFC.** (A) *Left*, Pie chart showing percentage of mPFC neurons classified as +HR encoders, -HR encoders, and HR non-encoders. *Right*, Pie chart showing the proportion of mPFC neurons classified as +HRV encoders, -HRV encoders, and HRV non-encoders, (n = 8 mice, 644 neurons).

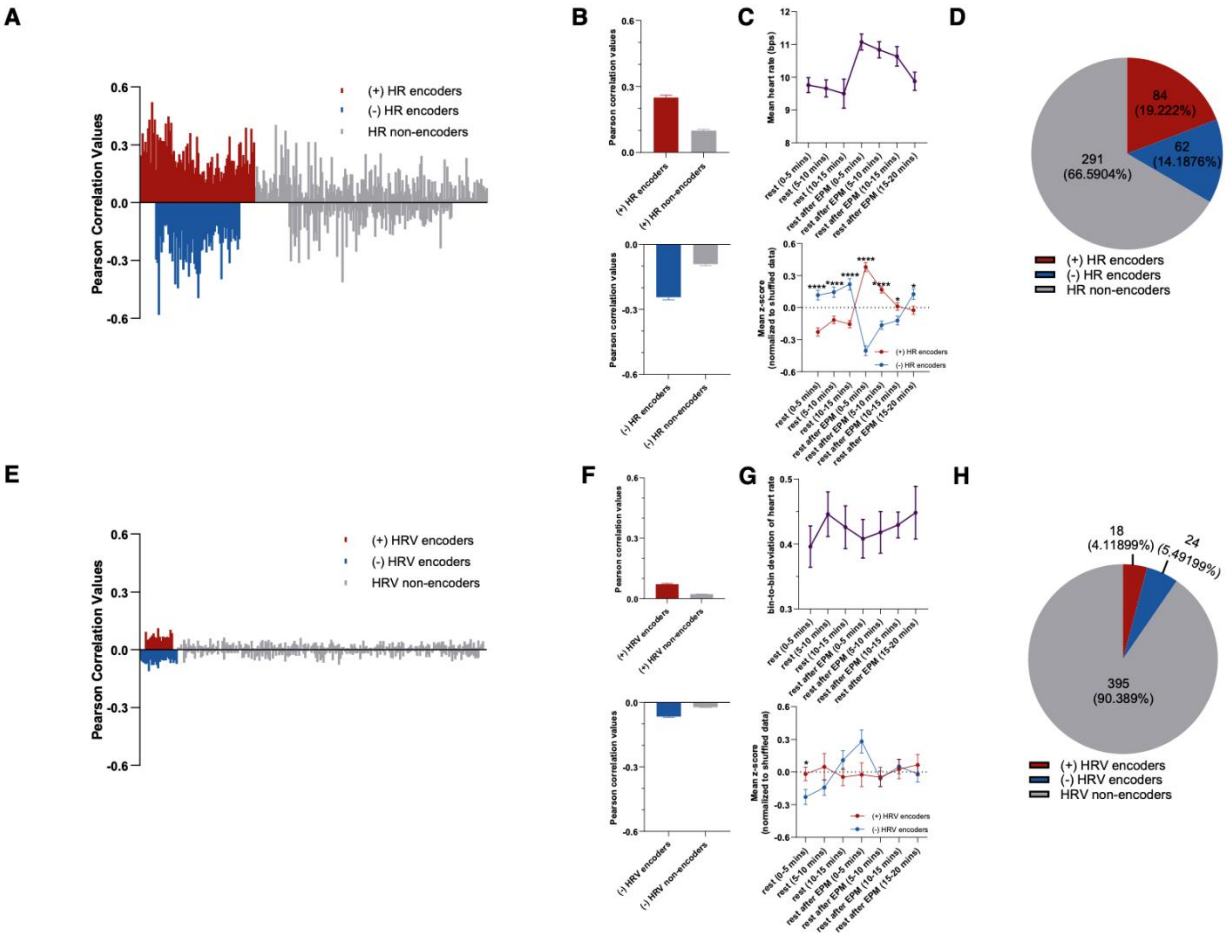


**Figure 2.4. Identification of neurocardiac networks in the mPFC using baseline periods before and after EPM exploration. (**A) Distribution showing the Pearson correlation values between calcium activity of individual neurons and heart rate during resting periods. Neurons with significantly positive correlations were classified as +HR encoders, and those with significantly negative correlations were classified as -HR encoders. Neurons whose correlation values did not exceed the 95th or fall below the 5th percentile of a shuffled null distribution were classified as HR non-encoders. (B) Bar graphs displaying mean Pearson correlation values between calcium activity and heart rate for each neural population. *Top*, Comparison between +HR encoders and HR non-encoders with positive correlation values. *Bottom*, Comparison between -HR encoders and HR non-encoders with negative correlation values. (C) *Top*, Mean heart rate across resting periods before behavior and during resting periods following EPM exploration. Heart rate increased during resting periods following EPM exploration and gradually returned toward baseline levels. *Bottom*, Mean z-scored activity of +HR encoders and -HR encoders across the same resting periods as (*Top*). (D) Pie chart showing percentage of mPFC neurons classified as +HR encoders, -HR encoders, and HR non-encoders. (E) Distribution showing the Pearson correlation values between calcium activity of individual neurons and HRV during resting periods. Neurons with significantly positive correlations were classified as +HRV encoders, and those with significantly negative correlations were classified as -HRV encoders. Neurons whose correlation values did not exceed the 95th or fall below the 5th percentile of a shuffled null distribution were classified as HRV non-encoders. (Figure caption continued on the next page)

(Figure caption continued from the previous page) (F) Bar graphs displaying mean Pearson correlation values between calcium activity and heart rate for each neural population. *Top*, Comparison between +HRV encoders and HRV non-encoders with positive correlation values. *Bottom*, Comparison between -HRV encoders and HRV non-encoders with negative correlation values. (G) *Top*, Mean HRV across resting periods before behaviors and during resting periods following EPM exploration. HRV shows moderate fluctuations during resting periods without significant changes. *Bottom*, Mean z-scored activity of +HRV encoders and -HRV encoders across the same resting periods as (*Top*). Data are shown as mean ± SEM. *$p < 0.05$, ****$p < 0.0001$, (n = 6 mice, 437 neurons).

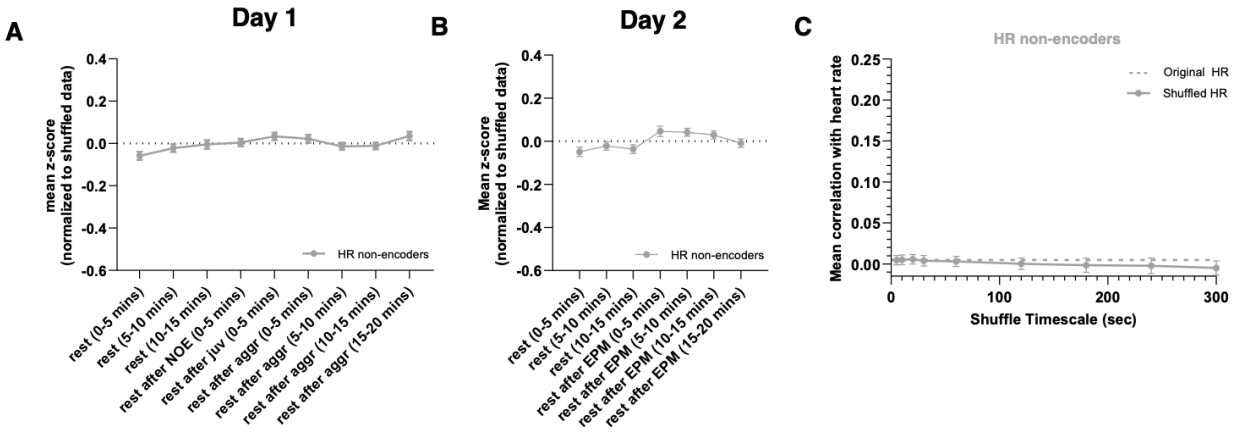


**Figure 2.5. HR non-encoders are unresponsive to spontaneous changes in heart rate.** (A) Mean z-scored calcium activity of HR non-encoders across resting periods before behavior and during resting periods following NOE, social interactions with a juvenile (juv), and exposure to an aggressor (aggr). These recordings were performed the first day of experiments (i.e., Day 1) (n = 8 mice, 644 neurons). (B) Mean z-scored calcium activity of HR non-encoders across resting periods before behavior and during resting periods following EPM exploration. These recordings were performed the second day of experiments (i.e., Day 2) (n = 6 mice, 437 neurons). (C) Mean correlation of HR non-encoders with heart rate across increasing temporal shuffling windows (n = 8 mice, 644 neurons). Dashed gray line indicates the correlation with unshuffled heart rate. Data are shown as mean ± SEM.

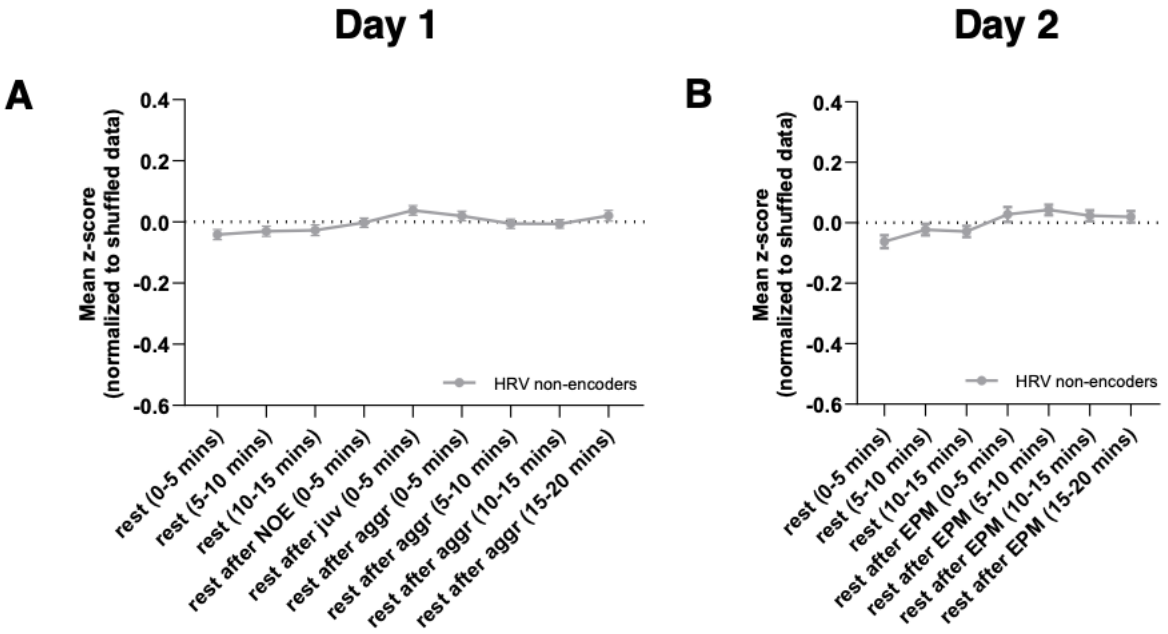


**Figure 2.6. HRV non-encoders are unresponsive to spontaneous changes in HRV.** (A) Mean z-scored calcium activity of HRV non-encoders across resting periods before behavior and during resting periods following NOE, social interactions with a juvenile (juv), and exposure to an aggressor (aggr). These recordings were performed the first day of experiments (i.e., Day 1) (n = 8 mice, 644 neurons). (B) Mean z-scored calcium activity of HRV non-encoders across resting periods before behavior and during resting periods following EPM exploration. These recordings were performed the second day of experiments (i.e., Day 2) (n = 6 mice, 437 neurons). Data are shown as mean ± SEM.

## 2.6 References


1. Engelhardt, E. (2018). Cerebral localization of the mind and higher functions The beginnings. *Dementia & neuropsychologia*, *12*(3), 321-325.
2. Ziskind, B., & Halioua, B. (2004). Concepts of the heart in Ancient Egypt. *Medecine Sciences: M/S*, *20*(3), 367-373.
3. Brandt, T., & Huppert, D. (2021). Brain beats heart: a cross-cultural reflection. *Brain*, *144*(6), 1617-1620.
4. Azzalini, D., Buot, A., Palminteri, S., & Tallon-Baudry, C. (2021). Responses to heartbeats in ventromedial prefrontal cortex contribute to subjective preference-based decisions. *Journal of Neuroscience*, *41*(23), 5102-5114.
5. Hsueh, B., Chen, R., Jo, Y., Tang, D., Raffiee, M., Kim, Y. S., ... & Deisseroth, K. (2023). Cardiogenic control of affective behavioural state. *Nature*, *615*(7951), 292-299.
6. Yoshimoto, A., Morikawa, S., Kato, E., Takeuchi, H., & Ikegaya, Y. (2024). Top-down brain circuits for operant bradycardia. *Science*, *384*(6702), 1361-1368.
7. Sakaki, M., Yoo, H. J., Nga, L., Lee, T. H., Thayer, J. F., & Mather, M. (2016). Heart rate variability is associated with amygdala functional connectivity with MPFC across younger and older adults. *Neuroimage*, *139*, 44-52.
8. Dinç, F., Inan, H., Hernandez, O., Schmuckermair, C., Hazon, O., Tasci, T., ... & Schnitzer, M. J. (2021). Fast, scalable, and statistically robust cell extraction from large-scale neural calcium imaging datasets. *BioRxiv*, 2021-03.

9. Corder, G., Ahanonu, B., Grewe, B. F., Wang, D., Schnitzer, M. J., & Scherrer, G. (2019). An amygdalar neural ensemble that encodes the unpleasantness of pain. *Science*, *363*(6424), 276-281.
10. Adhikari, A., Lerner, T. N., Finkelstein, J., Pak, S., Jennings, J. H., Davidson, T. J., ... & Deisseroth, K. (2015). Basomedial amygdala mediates top-down control of anxiety and fear. *Nature*, *527*(7577), 179-185.
11. Azzalini, D., Buot, A., Palminteri, S., & Tallon-Baudry, C. (2021). Responses to heartbeats in ventromedial prefrontal cortex contribute to subjective preference-based decisions. *Journal of Neuroscience*, *41*(23), 5102-5114.
12. Park, H. D., Correia, S., Ducorps, A., & Tallon-Baudry, C. (2014). Spontaneous fluctuations in neural responses to heartbeats predict visual detection. *Nature neuroscience*, *17*(4), 612-618.

# Chapter 3 – Prefrontal neurocardiac networks during beta-adrenergic overstimulation

## 3.1 Introduction

In the previous chapter, we identified distinct subpopulations of mPFC neurons that differentially encode spontaneous fluctuations in heart rate in freely moving mice. These neurocardiac networks included neurons that were positively correlated, negatively correlated, or uncorrelated with heart rate dynamics, suggesting a heterogeneous and structured representation of cardiac signals within the mPFC. However, whether these neural populations are sensitive to changes in autonomic state (such as those driven by sympathetic activation) remained unknown. To address this question, we sought to test how HR encoders respond to a controlled pharmacological manipulation of cardiac function. We used isoproterenol (iso), a synthetic beta-adrenergic agonist that selectively stimulates beta1 and beta2-adrenergic receptors, mimicking the effects of sympathetic nervous system activation.[1] Iso increases heart rate and cardiac contractility by enhancing pacemaker activity and promoting calcium influx in cardiomyocytes.[2,3]

A recent study in humans with generalized anxiety disorder demonstrated that peripheral beta-adrenergic stimulation with iso not only heightened cardiac and interoceptive responses but also led to blunted activity in the vmPFC.[4] Importantly, reduced vmPFC activation was associated with exaggerated heart rate reactivity and increased anxiety ratings, suggesting that excessive adrenergic input can suppress prefrontal encoding of bodily states even in the absence of task demands.[4]

In this chapter, we administered a single intraperitoneal dose of iso (5 mg/kg) and simultaneously recorded heart rate and calcium activity from mPFC neurons in freely moving mice. We aimed to determine (1) whether HR encoders are modulated by peripheral sympathetic stimulation and (2) whether the structure or stability of neurocardiac representations changes in the context of pharmacologically induced tachycardia. We hypothesized that pharmacologically increasing heart rate using iso would differentially modulate these populations: specifically, +HR encoders would significantly increase their activity, -HR encoders would significantly decrease their activity, and HR non-encoders would remain unaffected – reflecting a preserved encoding of elevated cardiac output. Interestingly, we found that iso induced a sustained elevation in heart rate in mice, but paradoxically suppressed the dynamic activity of HR encoders. Neurons that previously tracked moment-to-moment fluctuations in heart rate became less responsive under iso, suggesting a flattening of neurocardiac encoding during heightened sympathetic drive. These findings indicate that the fidelity of heart rate representation in the mPFC is not static but is dependent on the peripheral autonomic state – potentially reflecting a saturation or active interference mechanism that can become during periods of elevated physiological arousal.

## 3.2 Materials and Methods

### Animal Subjects

All animal care procedures and experiments were conducted in accordance with the National Institutes of Health guidelines and approved by the Administrative Panels on Laboratory Animal Care at the University of California, San Francisco. Mice were

housed in a temperature-controlled environment (22–24 °C) with ad libitum access to food and water. Mice were reared in normal lighting conditions (12-h light/dark cycle). Male C57BL/6J mice (10-12 weeks old at the time of the microendoscopic surgery and 14-16 weeks at the time of the ECG surgery) were used.

**Surgical Procedures**

All animals used for experiments underwent a two-stage surgical protocol: one for viral delivery/GRIN lens implantation and another for implantation of ECG wires. During both procedures, mice were anesthetized with isoflurane delivered in 95% oxygen at a flow rate of 0.9 L/min. For viral delivery/GRIN lens implantation, animals were placed in a stereotaxic apparatus (David Kopf Instruments) using head bars for head fixation. Subcutaneous injections of Ethiqa XR (3.25 mg/kg) and meloxicam (2 mg/kg) were administered at the onset of surgery for analgesia. Body temperature was maintained with a heating pad throughout the procedure. The local anesthetic lidocaine was injected in the incision site and a midline incision was made along the scalp to expose the skull, which was aligned using bregma and lambda. Following surgery, animals were kept on a heating pad for recovery until fully ambulatory. A second dose of meloxicam was administered the day after surgery. For implantation of ECG wires, animals were anesthetized using an anesthesia face mask (Kent Scientific) and placed on a heating pad to maintain body temperature. Subcutaneous injections of Ethiqa XR (3.25 mg/kg) and meloxicam (2 mg/kg) were administered at the onset of surgery for analgesia. The local anesthetic lidocaine was injected in the incision site and a midline incision was made along the chest to expose the chest muscles. Following surgery,

animals were kept on a heating pad for recovery until fully ambulatory. A second dose of meloxicam and 1 mL of sterile saline was administered the day after surgery.

Viral injections and GRIN lens implantation were carried out in mice aged 10-12 weeks old. A 0.6 mm craniotomy was made above the right mPFC at coordinates +1.7 mm AP and +0.3 mm ML relative to bregma using a dental drill. The viral construct AAV9-hSyn-jGCaMP7f-WPRE (AddGene) was diluted 1:3 in sterile saline prior to injection. Using a 35-gauge syringe (World Precision Instruments) connected to a UMP3 UltraMicroPump, 150 nL of virus was infused at four depths (-2.00 mm, -2.25 mm, -2.50 mm, -2.75 mm DV) at a flow rate of 150 nL/min. The syringe remained in place for five minutes following each injection to prevent backflow. After five minutes, the syringe was slowly removed from the brain and a GRIN lens implantation was performed. A 0.5 mm x 4.0 mm GRIN lens (Inscopix) was lowered through the 0.6 mm craniotomy to a depth of -2.3 mm and secured to the skull using Metabon (Parkell). Postoperatively, mice were singly housed and given four weeks to recover before performing the ECG surgery.

ECG surgeries were carried out in mice aged 14-16 weeks old that were implanted with GRIN lenses. Four perfluoroalkoxy-coated stainless steel wires (791000, A-M Systems) soldered to a 8-pin mouse headmount (8415-SM, Pinnacle Technology) were tunneled through the back of the mouse until they reach the chest. The wires were secured on the chest muscles with non-absorbable sutures while making sure the recording site of each wire did not contact each other. From the four stainless steel wires, two of the wires pick up ECG signal, one wire was the ground, and one wire provide additional

support to diminish movement artifacts. After suturing the wires to the chest muscles, the incision was closed with sutures. Then, the animals were placed in the stereotaxic apparatus and the headmount was secured to the skull with metabond and dental acrylic (Ortho-Jet, Patterson Dental). Postoperatively, mice were singly housed and given at least four days to recover before performing experiments.

After experiments, mice were intracardially perfused with 4% PFA to verify GRIN lens placement and the injection site of the viral construct in the mPFC.

**Behavioral Tasks**

Mice underwent a habituation period to acclimate them to the head-mounted microscope over the course of 2 weeks. Additionally, they were habituated to experimenter handling for four consecutive days, with each session lasting 10 minutes. On testing days, mice were transported to the behavioral room 1 hour prior to the start of the experiment to allow for acclimation. Before the beginning of the experiment, the animals were plugged to the head-mounted microscope and the ECG pre-amplifier for 20 minutes and left undisturbed to allow recovery from the brief stress associated with handling and equipment attachment.

*Pharmacology*

Before pharmacological manipulations on the first day, mice were recorded during a 15 minute of baseline period, followed by NOE (5 min), a rest period (5 min), interaction with a juvenile mouse (10 min), another rest period (5 min), interaction with a CD1

aggressor (20 min), a final rest period (20 min), followed by an injection of saline or 5 mg/kg of iso (Tocris) in the home cage (45 min). On the second day, mice were recorded during a 15 minute baseline period, followed by EPM (15 minutes), a rest period (20 min), and during another response to saline or 5 mg/kg iso injection (45 min).

**Data Acquisition and Processing**

Calcium signals were imaged at 20 Hz with 4x downsampling using a head-mounted 1-photon microendoscope (nVoke2, Inscopix Inc.). Calcium videos were preprocessed using IDPS, including spatial band-pass filtering with cutoffs set to 0.008 pixel-1 (low) and 0.500 pixel-1 (high), followed by motion correction. Preprocessed calcium videos were exported from IDPS as NWB files, converted to HDF5 format using HDFView, and then imported into MATLAB for cell segmentation. Putative cellular ROIs were identified and DF/F signals were extracted using EXTRACT.[5] For each calcium movie, putative neurons were manually curated to remove ROIs with low signal-to-noise ratio or overlapping boundaries. Cell sorting was done with the assistance of the signalSorter GUI from the open-source calcium imaging analysis package (CIAPKG).[6] Calcium signal (DF/F) from each neuron was averaged in 1-second segments.

ECG signals were acquired at 10 KHz using a head-mounted 4-channel mouse preamplifier (8406-SE4, Pinnacle Technology) connected to a 9-pin commutator (8401-HS, Pinnacle Technology) from the data acquisition system. Signals were filtered with a high-pass cutoff of 10 Hz and a low-pass cutoff between 200-300 Hz. Preprocessed ECG recordings were exported from Sirenia software as EDF files and subsequently

imported into MATLAB for further analysis. ECG data were converted from frames to seconds. Segments with motion artifacts were manually curated or excluded if the signal was significantly distorted. Custom MATLAB code was used to detect R-peaks, corresponding to individual heartbeats, from the ECG signal. Heart rate was calculated as the sum of R-peaks in 1-second segments. HRV was calculated as the bin-to-bin deviations in heart rate (using standard deviation calculations). Specifically, HRV was computed as the difference in heart rate between consecutive 1-second bins. Behavioral videos were recorded at 25 frames per second using Sirenia software. A TTL cable connecting the data acquisition system with the Inscopix DAQ box was used to temporally align the behavioral videos with ECG signals and calcium imaging data.

**Data Analysis**

All analyses of calcium activity and ECG signal were performed using code written in MATLAB. The baseline period was defined as the 15 minutes prior to saline or iso injections.

*Mean activity of neurocardiac networks during pharmacological manipulations*

To calculate each neuron's (i.e., +HR encoders, -HR encoders, and HR non-encoders) mean activity during saline or iso injections, we first averaged the DF/F signal into 1-second segments. We then computed the mean activity as a z-score, normalized relative to the shuffled DF/F signal.

## 3.3 Results

To investigate how prefrontal neurocardiac networks respond to increases in sympathetic tone, we pharmacologically stimulated the beta-adrenergic system using intraperitoneal injections of iso (5 mg/kg), a non-selective beta-adrenoreceptor agonist known to elicit tachycardia (**Figure 3.1 A**). As a control, a subset of mice received saline injections. In both groups, we performed simultaneous calcium imaging and ECG recordings while animals remained freely moving. We quantified the average heart rate (in beats per second) before and after injection and observed that saline injection did not significantly alter mean heart rate relative to baseline (**Figure 3.1B, top panel**). In contrast, iso injection produced a robust and sustained increase in heart rate across animals (**Figure 3.1B, bottom panel**), confirming effective activation of the peripheral beta-adrenergic system.

We next assessed how pharmacologically elevated heart rate influenced HR encoders in the mPFC. First, we examined the effect of saline injection on average heart rate and neural activity across a 45-minute period. As expected, saline induce small changes in mean heart rate over time (**Figure 3.1C, top panel**). However, both +HR encoders and -HR encoders remained responsive, exhibiting dynamic activity patterns similar to resting periods. Specifically, +HR encoders increased their activity significantly when -HR encoders decreased theirs, and vice versa (**Figure 3.1C, middle panel**). These changes were consistent across multiple time bins and significantly above what would be expected by chance, as determined by z-scoring relative to shuffled data. HR non-encoders did not exhibit any significant modulation (**Figure 3.1C, bottom panel**).

In contrast, iso induced a rapid and sustained elevation in mean heart rate that persisted for the entire 45-minutes post-injection period (**Figure 3.1D, top panel**). Surprisingly, this increase in sympathetic tone led to a blunting of HR encoder dynamics. Despite the persistent elevation in heart rate, +HR encoders failed to produce a similar elevation in activity; rather, their z-scored activity remained closed to the baseline (corresponding to a z-score ~0; **Figure 3.1D, middle panel**). Likewise, -HR encoders exhibited limited changes in activity. These results indicate a disruption in the temporal fidelity of heart rate encoding in mPFC neurons during periods of heightened sympathetic drive. During this period there was no overall change in the activity of HR non-encoders (**Figure 3.1D, bottom panel**).

## 3.4 Discussion

In this chapter, we investigated whether prefrontal neurocardiac networks remain responsive to cardiac fluctuations under conditions of elevated sympathetic tone. By administering the beta-adrenergic agonist iso, we pharmacologically induced a sustained increase in heart rate and tested whether mPFC neurons that previously tracked moment-to-moment cardiac dynamics under resting conditions preserved their functional properties in this altered physiological state. We found that while iso reliably increased heart rate across animals, it paradoxically disrupted the activity patterns of both +HR and -HR encoders, flattening their responses and diminishing the fidelity of heart rate representation in the mPFC. These findings indicate that the encoding of heart rate by prefrontal circuits is not fixed but instead dynamically modulated by the autonomic system.

The observed blunting of HR encoder activity in response to iso was unexpected, particularly given our initial hypothesis that sympathetic stimulation would engage and potentially amplify the directionally tuned responses of HR encoders. Notably, we did not observe a clear initial increase in +HR encoder activity or decrease in -HR encoder activity at the onset of heart rate acceleration. Instead, despite sustained elevations in heart rate, fluctuations in both +HR and -HR encoder activity were significantly dampened throughout the iso response. This compression of encoding fidelity suggests a decoupling between heart rate dynamics and mPFC neural activity. One possibility is that under conditions of maximal sympathetic drive, prefrontal circuits experience an interference or gating effect, shifting processing priorities away from ongoing visceral monitoring. In this state, neurons may become functionally disengaged from heart rate tracking, potentially reflecting a broader reorganization of neurocardiac integration during high-arousal states.

Another possible explanation for this flattening of neurocardiac dynamics is that beta-adrenergic activation alters the gain or input sensitivity of mPFC neurons, either directly via central adrenergic signaling or indirectly through changes in interoceptive feedback pathways. Although iso primarily acts peripherally, beta-adrenergic receptors are expressed in central autonomic regions, including the mPFC, and may mediate local neuromodulatory effects. Alternatively, the suppression of encoding may reflect a functional decoupling of the mPFC from afferent cardiac signals during high-arousal states, possibly as part of a broader network reorganization prioritizing behavioral or contextual processing over visceral monitoring. Future experiments targeting central

adrenergic pathways, or combining pharmacology with behavioral manipulations, may help disentangle these mechanisms.

Importantly, the flattening of encoder activity was not observed following saline injection, which served as a critical control for potential confounds related to handling, injection stress, or time-dependent drift. Following saline injection, HR encoders preserved their dynamic fluctuations in activity, and HR non-encoders remained unresponsive. This contrast highlights the sensitivity of neurocardiac networks to shifts in autonomic state and reinforces the idea that mPFC representations of heart rate are not merely reflexible, but context-dependent.

Together, these findings reveal a fundamental constraint in the stability of neurocardiac representations under conditions of physiological arousal. While prefrontal neurocardiac networks are capable of robustly tracking real-time cardiac signals during baseline or mildly perturbed states, their encoding fidelity diminishes when the system is driven into a hyperadrenergic regime. This raises the possibility that neurocardiac coupling in the mPFC may function optimally within a specific range of autonomic inputs and may be selectively downregulated outside of this range to enable alternative computational priorities. More broadly, these results underscore the importance of considering physiological states as a critical variable when interpreting interoceptive coding in higher-order brain regions.

## 3.5 Figures

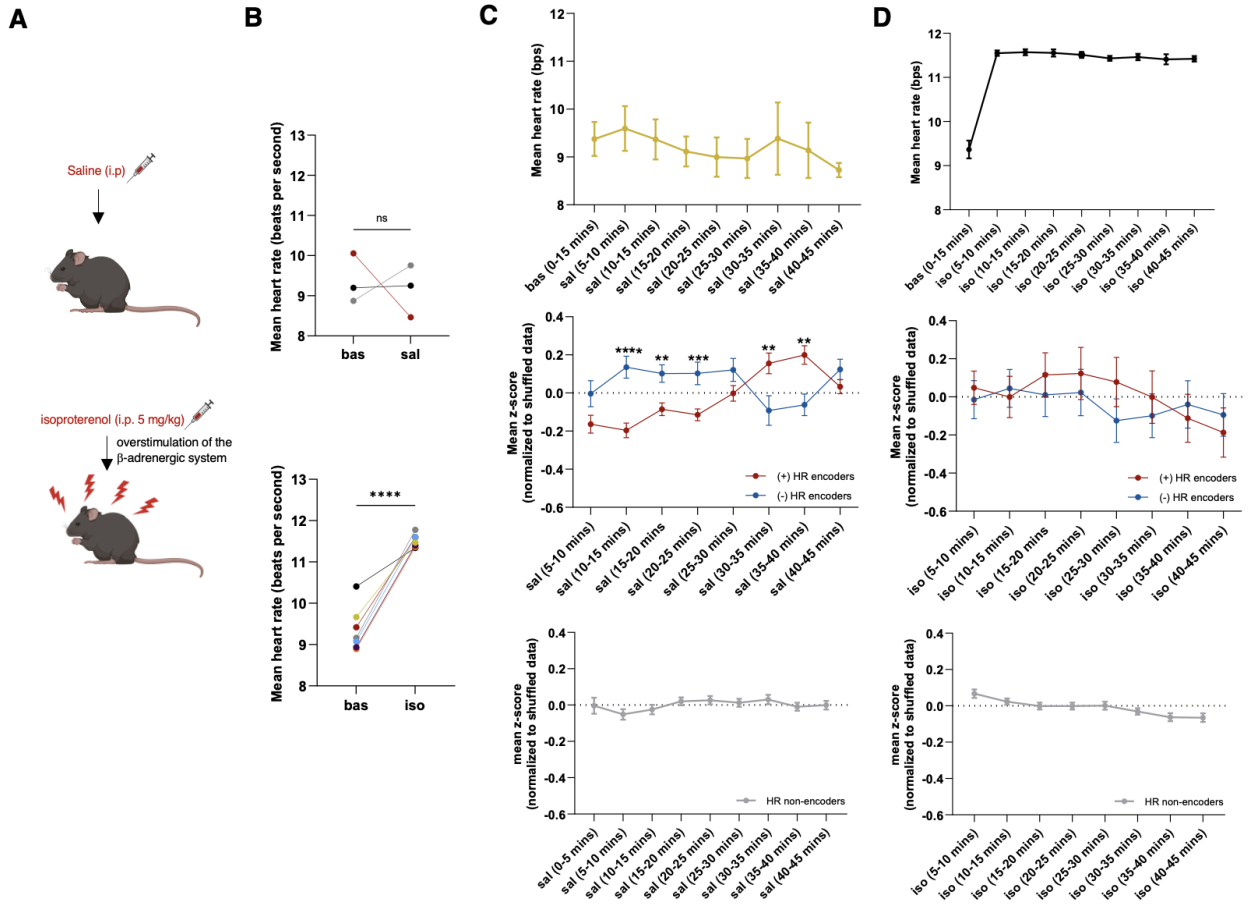


**Figure 3.1. Prefrontal neurocardiac networks are decoupled from heart rate during beta-adrenergic overstimulation.** (A) Schematic showing intraperitoneal (i.p.) injection of saline (*top*) or iso (*bottom*), a beta-adrenergic agonist that increases sympathetic drive. The red symbols around the mouse indicate heightened arousal. (B) Mean heart rate during baseline (bas) and after injection of saline (sal) (*top*) (n = 3 mice) or iso (*bottom*) (n = 7 mice) across animals. (C) *Top*, Mean heart rate during baseline and after saline injection. *Middle*, Mean z-scored activity of +HR encoders and -HR encoders following saline injection. *Bottom*, Mean z-scored activity of HR non-encoders following saline injection (n = 3 mice, 261 neurons). (D) *Top*, Mean heart rate during baseline and after iso injection. *Middle*, Mean z-scored activity of +HR encoders and -HR encoders following iso injection. *Bottom*, Mean z-scored activity of HR non-encoders following iso injection (n = 6 mice, 472 neurons). Data are shown as mean ± SEM. **p < 0.01, ***p < 0.001, ****p < 0.0001.

## 3.6 References


1. Weitl, N., & Seifert, R. (2008). Distinct interactions of human β1-and β2-adrenoceptors with isoproterenol, epinephrine, norepinephrine, and dopamine. *The Journal of pharmacology and experimental therapeutics*, *327*(3), 760-769.
2. DiFrancesco, D. (2010). The role of the funny current in pacemaker activity. *Circulation research*, *106*(3), 434-446.
3. Bean, B. P., Nowycky, M. C., & Tsien, R. W. (1984). β-Adrenergic modulation of calcium channels in frog ventricular heart cells. *Nature*, *307*(5949), 371-375.
4. Teed, A. R., Feinstein, J. S., Puhl, M., Lapidus, R. C., Upshaw, V., Kuplicki, R. T., ... & Khalsa, S. S. (2022). Association of generalized anxiety disorder with autonomic hypersensitivity and blunted ventromedial prefrontal cortex activity during peripheral adrenergic stimulation: a randomized clinical trial. *JAMA psychiatry*, *79*(4), 323-332.
5. Dinç, F., Inan, H., Hernandez, O., Schmuckermair, C., Hazon, O., Tasci, T., ... & Schnitzer, M. J. (2021). Fast, scalable, and statistically robust cell extraction from large-scale neural calcium imaging datasets. *BioRxiv*, 2021-03.
6. Corder, G., Ahanonu, B., Grewe, B. F., Wang, D., Schnitzer, M. J., & Scherrer, G. (2019). An amygdalar neural ensemble that encodes the unpleasantness of pain. *Science*, *363*(6424), 276-281.

# Chapter 4 – Prefrontal neurocardiac networks during approach-avoidance behaviors

## 4.1 Introduction

In the previous chapter, we demonstrated that prefrontal neurocardiac networks dynamically encode spontaneous heart rate fluctuations under baseline and saline conditions but exhibit a striking loss of temporal fidelity during pharmacologically induced sympathetic activation. These findings suggest that the ability of mPFC neurons to track cardiac signals is not static but is modulated by the organism's autonomic state. However, it remains unclear whether these neurocardiac representations are behaviorally relevant – particularly during naturalistic behaviors that involve internal conflicts between exploration and threat avoidance.

Approach-avoidance behaviors are critical for survival, as they require the integration of competing motivational drives: the desire to explore novel or socially salient stimuli and the need to avoid potential threats or anxiety-provoking contexts. These behaviors recruit both peripheral autonomic responses and higher-order cognitive processing, providing a unique window into the interplay between physiological arousal and prefrontal encoding.[1,2] Previous studies have shown that heart rate changes robustly during approach and avoidance behaviors, often reflecting anticipatory arousal or evaluative processes.[1-3] However, whether prefrontal neurocardiac networks encode these rapid cardiac fluctuations during behaviorally salient decisions, and whether such encoding differs across social and anxiety-related contexts, remains unknown.

To address these questions, we investigated the activity of mPFC HR encoders during three distinct approach-avoidance paradigms: (1) social exploration of either a juvenile conspecific or a CD1 aggressor, (2) exploration of a novel object, and (3) exploration of the EPM, a classic assay of anxiety-like behavior. Social interactions with a juvenile mouse typically elicit approach behavior, whereas interactions with a CD1 aggressor evoke competing approach and avoidance drives. Similarly, transitions between open and closed arms in the EPM provide a well-established model of anxiety-related approach-avoidance conflicts. In contrast, novel object exploration offers a context of low social and physical threat, allowing for the investigation of curiosity-driven approach behaviors with minimal anxiety-related avoidance. By combining simultaneous calcium imaging and ECG recordings in freely moving mice during these tasks, we aimed to test whether prefrontal neurocardiac networks exhibit distinct patterns of activity during approach and avoidance episodes and whether these patterns are preserved across contexts.

Based on our prior findings, we hypothesized that +HR encoders and -HR encoders would exhibit directionally tuned activity during moments of behavioral engagement, reflecting the dynamic tracking of cardiac fluctuations associated with approach and avoidance behaviors. We further predicted that the strength of neurocardiac coupling would vary across social and anxiety-related contexts, potentially revealing specialized subcircuits within the mPFC that differentially process interoceptive signals during social versus anxiogenic encounters.

This chapter provides evidence that prefrontal neurocardiac networks are not only sensitive to spontaneous changes in heart rate but also actively track cardiac dynamics during complex behaviors that require balancing competing motivational states. Our findings reveal that the fidelity of neurocardiac encoding is preserved during social approach-avoidance behaviors but can be selectively attenuated during social and anxiogenic contexts that promote high avoidance, highlighting a flexible and context-dependent integration of interoceptive signals in the prefrontal cortex.

## 4.2 Materials and Methods

### Animal Subjects

All animal care procedures and experiments were conducted in accordance with the National Institutes of Health guidelines and approved by the Administrative Panels on Laboratory Animal Care at the University of California, San Francisco. Mice were housed in a temperature-controlled environment (22–24 °C) with ad libitum access to food and water. Mice were reared in normal lighting conditions (12-h light/dark cycle). Male C57BL/6J mice (10-12 weeks old at the time of the microendoscopic surgery and 14-16 weeks at the time of the ECG surgery) were used.

### Surgical Procedures

All animals used for experiments underwent a two-stage surgical protocol: one for viral delivery/GRIN lens implantation and another for implantation of ECG wires. During both procedures, mice were anesthetized with isoflurane delivered in 95% oxygen at a flow rate of 0.9 L/min. For viral delivery/GRIN lens implantation, animals were placed in a stereotaxic apparatus (David Kopf Instruments) using head bars for head fixation.

Subcutaneous injections of Ethiqa XR (3.25 mg/kg) and meloxicam (2 mg/kg) were administered at the onset of surgery for analgesia. Body temperature was maintained with a heating pad throughout the procedure. The local anesthetic lidocaine was injected in the incision site and a midline incision was made along the scalp to expose the skull, which was aligned using bregma and lambda. Following surgery, animals were kept on a heating pad for recovery until fully ambulatory. A second dose of meloxicam was administered the day after surgery. For implantation of ECG wires, animals were anesthetized using an anesthesia face mask (Kent Scientific) and placed on a heating pad to maintain body temperature. Subcutaneous injections of Ethiqa XR (3.25 mg/kg) and meloxicam (2 mg/kg) were administered at the onset of surgery for analgesia. The local anesthetic lidocaine was injected in the incision site and a midline incision was made along the chest to expose the chest muscles. Following surgery, animals were kept on a heating pad for recovery until fully ambulatory. A second dose of meloxicam and 1 mL of sterile saline was administered the day after surgery.

Viral injections and GRIN lens implantation were carried out in mice aged 10-12 weeks old. A 0.6 mm craniotomy was made above the right mPFC at coordinates +1.7 mm AP and +0.3 mm ML relative to bregma using a dental drill. The viral construct AAV9-hSyn-jGCaMP7f-WPRE (AddGene) was diluted 1:3 in sterile saline prior to injection. Using a 35-gauge syringe (World Precision Instruments) connected to a UMP3 UltraMicroPump, 150 nL of virus was infused at four depths (-2.00 mm, -2.25 mm, -2.50 mm, -2.75 mm DV) at a flow rate of 150 nL/min. The syringe remained in place for five minutes following each injection to prevent backflow. After five minutes, the syringe was slowly

removed from the brain and a GRIN lens implantation was performed. A 0.5 mm x 4.0 mm GRIN lens (Inscopix) was lowered through the 0.6 mm craniotomy to a depth of -2.3 mm and secured to the skull using Metabon (Parkell). Postoperatively, mice were singly housed and given four weeks to recover before performing the ECG surgery.

ECG surgeries were carried out in mice aged 14-16 weeks old that were implanted with GRIN lenses. Four perfluoroalkoxy-coated stainless steel wires (791000, A-M Systems) soldered to a 8-pin mouse headmount (8415-SM, Pinnacle Technology) were tunneled through the back of the mouse until they reach the chest. The wires were secured on the chest muscles with non-absorbable sutures while making sure the recording site of each wire did not contact each other. From the four stainless steel wires, two of the wires pick up ECG signal, one wire was the ground, and one wire provide additional support to diminish movement artifacts. After suturing the wires to the chest muscles, the incision was closed with sutures. Then, the animals were placed in the stereotaxic apparatus and the headmount was secured to the skull with metabond and dental acrylic (Ortho-Jet, Patterson Dental). Postoperatively, mice were singly housed and given at least four days to recover before performing experiments.

After experiments, mice were intracardially perfused with 4% PFA to verify GRIN lens placement and the injection site of the viral construct in the mPFC.

**Behavioral Tasks**

Mice underwent a habituation period to acclimate them to the head-mounted microscope over the course of 2 weeks. Additionally, they were habituated to experimenter handling for four consecutive days, with each session lasting 10 minutes. On testing days, mice were transported to the behavioral room 1 hour prior to the start of the experiment to allow for acclimation. Before the beginning of the experiment, the animals were plugged to the head-mounted microscope and the ECG pre-amplifier for 20 minutes and left undisturbed to allow recovery from the brief stress associated with handling and equipment attachment.

*NOE task*

To assess exploratory behavior and novelty recognition, mice were subjected to a NOE assay. The NOE test was performed in the mouse home cage containing a single object (e.g., lego toys or falcon tube). Mice were gently placed in the wall opposite to the novel object location and were allowed to freely explore for 5 minutes. The objects were positioned in a fixed location within the home cage to standardize testing conditions across animals.

Exploration of the novel object was defined as direct interaction with the object, accompanied by active sniffing or touching of the object. Avoidance behavior included time spent distant from the novel object.

*Social behaviors*

To evaluate social approach and avoidance behaviors, mice were tested in two distinct social interaction assays: one involving a non-aggressive juvenile conspecific and another involving an aggressive CD1 mouse. The assay was performed in the mouse home cage.

For the juvenile interaction assay, a novel, juvenile mouse (3-5 weeks old, sex-matched) was enclosed within a wire cup placed at one end of the arena. Experimental mice were placed opposite to the wire cup location and allowed to explore freely for 10 minutes. Specifically, approach toward the social stimulus was defined as periods when the mouse was near the wire cup and oriented toward the conspecific, with or without direct sniffing. Avoidance behavior included time spent distant from the conspecific's wire cup in the social task.

In a separate assay, experimental mice were exposed to a novel, CD1 aggressor mouse (retired breeder, 4-6 months old, sex-matched) housed within a wire cup. The setup was identical to the juvenile assay. Mice were allowed to freely explore the CD1 aggressor for 20 minutes. approach toward the social stimulus was defined as periods when the mouse was near the wire cup and oriented toward the conspecific, with or without direct sniffing. Avoidance behavior included time spent distant from the conspecific's wire cup in the social task.

*Elevated Plus Maze*

To assess anxiety-like behavior, mice were tested in the EPM. The EPM apparatus consisted of two opposing open arms, two opposing closed arms, and a central zone connecting all four arms. Each mouse was placed in the center of the EPM and allowed to freely explore the maze for 15 minutes. An entry was defined as all four paws entering one of the EPM zones.

**Data Acquisition and Processing**

Calcium signals were imaged at 20 Hz with 4x downsampling using a head-mounted 1-photon microendoscope (nVoke2, Inscopix Inc.). Calcium videos were preprocessed using IDPS, including spatial band-pass filtering with cutoffs set to 0.008 pixel-1 (low) and 0.500 pixel-1 (high), followed by motion correction. Preprocessed calcium videos were exported from IDPS as NWB files, converted to HDF5 format using HDFView, and then imported into MATLAB for cell segmentation. Putative cellular ROIs were identified and DF/F signals were extracted using EXTRACT.[4] For each calcium movie, putative neurons were manually curated to remove ROIs with low signal-to-noise ratio or overlapping boundaries. Cell sorting was done with the assistance of the signalSorter GUI from the open-source calcium imaging analysis package (CIAPKG).[5] Calcium signal (DF/F) from each neuron was averaged in 1-second segments.

ECG signals were acquired at 10 KHz using a head-mounted 4-channel mouse preamplifier (8406-SE4, Pinnacle Technology) connected to a 9-pin commutator (8401-HS, Pinnacle Technology) from the data acquisition system. Signals were filtered with a

high-pass cutoff of 10 Hz and a low-pass cutoff between 200-300 Hz. Preprocessed ECG recordings were exported from Sirenia software as EDF files and subsequently imported into MATLAB for further analysis. ECG data were converted from frames to seconds. Segments with motion artifacts were manually curated or excluded if the signal was significantly distorted. Custom MATLAB code was used to detect R-peaks, corresponding to individual heartbeats, from the ECG signal. Heart rate was calculated as the sum of R-peaks in 1-second segments. HRV was calculated as the bin-to-bin deviations in heart rate (using standard deviation calculations). Specifically, HRV was computed as the difference in heart rate between consecutive 1-second bins. Behavioral videos were recorded at 25 frames per second using Sirenia software. A TTL cable connecting the data acquisition system with the Inscopix DAQ box was used to temporally align the behavioral videos with ECG signals and calcium imaging data.

**Data Analysis**

All analyses of calcium activity and ECG signal were performed using code written in MATLAB.

*Analysis of heart rate during behaviors*

Behavioral epochs were first identified, and the corresponding video frames were aligned with the ECG data. Heart rate was calculated by averaging the 1-second heart rate bins within each behavioral epoch. The mean heart rate for each mouse during each behavioral condition was then computed and plotted.

*Activity of neurocardiac networks during behaviors*

To quantify the activity of each neural population (+HR encoders, -HR encoders, and HR non-encoders) during behavior, DF/F calcium signal was first binned into 1-second segments. For each neuron, mean activity was calculated as a z-score normalized to a 5-minute resting baseline recorded prior to behavioral testing. The average of the mean z-scores for each neural population was then computed across all neurons identified in the study and plotted accordingly.

To assess real-time changes in neural population activity, z-scored DF/F signals were computed in 1-second bins, again normalized to the 5-minute pre-behavioral resting period. This analysis included all +HR encoders, -HR encoders, and HR non-encoders. For transitions in the EPM, we specifically calculated the difference in the average activity between the +HR encoders and the -HR encoders at two time points: 5 seconds before and 5 seconds after the transition. Activity of +HR encoders and -HR encoders was averaged across neurons within each mouse at these time points, and the difference between the two populations was then calculated.

*Correlation analysis between neurocardiac networks and heart rate during behaviors*

Pearson correlation coefficients were calculated between the activity of +HR encoders or -HR encoders and heart rate during behavioral epochs. This was performed by correlating the DF/F signal (binned in 1-second intervals) with heart rate values averaged over corresponding 1-second bins. Mean Pearson correlation values for all

+HR encoders and all -HR encoders identified in the study were then computed and plotted.

## 4.3 Results

We sought to determine whether prefrontal neurocardiac networks identified during baseline periods continue to track heart rate fluctuations during naturalistic approach-avoidance behaviors, and whether their engagement differs across social, non-social, and anxiety-related contexts. Furthermore, we aimed to test whether specific neurocardiac networks are recruited or suppressed when animals approach or avoid stimuli with different motivational valence. For example, it is possible that +HR encoders encode a variety of arousal states, such that they would be recruited during exploration of novel conspecifics, objects, and potentially anxiogenic spatial contexts. To address this, we performed simultaneous single-cell calcium imaging and ECG recordings in freely moving mice as they engaged in social interactions with a juvenile conspecific or a CD1 aggressor (**Figure 4.1C**, **Figure 4.1D**), explored a novel object (**Figure 4.2A**), and navigated the EPM (**Figure 4.3A**). We focused our analyses on the periods when animals were actively approaching or avoiding the social stimuli, the novel object, or when present in and transitioning between the different zones of the EPM. Specifically, approach toward the social stimulus was defined as periods when the mouse was near the wire cup and oriented toward the conspecific, with or without direct sniffing. Approach to the novel object was characterized by close proximity accompanied by active sniffing of the object. Avoidance behavior included time spent distant from the conspecific's wire cup in the social task or away from the novel object. For the EPM, we

analyzed epochs when the mouse was located in the open arms, closed arms, or the center zone, as well as transitions between these zones. Transitions were further categorized by their inferred emotional valence: open-to-open transitions reflected heightened exploratory behavior, closed-to-closed transitions indicated reduced exploration, closed-to-open transitions marked entry into a higher anxiety zone, and open-to-closed transitions marked retreat into a lower anxiety zone. For each of these defined behavioral events in the social and novel object tasks, we computed changes in heart rate and analyzed the activity of HR encoders by calculating the mean z-score of the DF/F signal, as well as the z-score in 1-second bins to capture real-time dynamics of neural activity during these behaviors. We also assessed the Pearson correlation between DF/F activity of HR encoders and heart rate to evaluate neurocardiac encoding. For the EPM, we similarly computed changes in heart rate, mean z-scored DF/F activity within each zone, and z-scored DF/F activity in 1-second bins aligned to EPM transitions. Additionally, we calculated the Pearson correlation between HR encoder activity and heart rate within each EPM zone to determine how the neurocardiac encoding varied across anxiety-related spatial contexts.

**Neurocardiac encoding during social exploration**

We first examined heart rate and prefrontal activity during social contexts. Across mice, heart rate significantly increased during both approach and avoidance episodes compared to baseline, with the highest heart rates observed during social approaches (**Figure 4.1A**). When directly comparing approach episodes, heart rates were highest during approach to the juvenile conspecific (**Figure 4.1A**). In contrast, when comparing

avoidance episodes, heart rates were highest when avoiding the CD1 aggressor (**Figure 4.1A**). These findings suggest that cardiac arousal during social interactions is sensitive to both the type of social stimulus and the animal's behavioral response. The elevated heart rates observed during approach to the juvenile conspecific likely reflect anticipatory arousal or social engagement, while the heightened heart rates during avoidance of the CD1 aggressor may indicate sustained physiological activation associated with threat perception and defensive behavior. This pattern highlights that heart rate responses are dynamically modulated by both the motivational context and the perceived level of social threat.

To specifically evaluate how prefrontal neurocardiac networks track cardiac dynamics during distinct social behaviors, we compared neural activity during approach and avoidance episodes toward the juvenile conspecific. During juvenile approach, +HR encoders significantly increased their activity relative to all neural populations, while -HR encoders significantly decreased their activity relative to all neural populations (**Figure 4.1B, left**). Time-aligned analyses confirmed that +HR encoders showed sustained elevated activity before and after the onset of approach episodes, whereas -HR encoders exhibited sustained suppression around these same transitions (**Figure 4.1D**). Consistent with these dynamics, overall positive correlations between neural activity and heart rate were observed for +HR encoders in approach epochs when the mouse was interacting with the juvenile mouse, while overall negative correlations were observed for -HR encoders during the same epochs (**Figure 4.1F, top left**). Interestingly, during avoidance of the juvenile, +HR encoders exhibited significantly elevated activity relative to all neural populations, but -HR encoders were not

significantly modulated relative to HR non-encoders (**Figure 4.1B, right**). During juvenile avoidance, the overall correlations between neurocardiac networks and heart rate remained intact, i.e., +HR encoders tended to be positively correlated with heart rate and had correlations that were significantly greater (more positive) than those of -HR encoders which tended to be negatively correlated with heart rate (**Figure 4.1F, top right**). This indicates that prefrontal neurocardiac coupling remains engaged even when animals temporarily disengage from the social target.

When mice interacted with the CD1 aggressor, +HR encoders increased their activity relative to all neural populations while -HR encoders exhibited no significant modulation relative to HR non-encoders (**Figure 4.1C, left**). Time-aligned analyses confirmed that +HR encoders showed a sustained elevation in activity both before and after the onset of approach episodes, whereas -HR encoders had decreased activity prior to, and at the time of the approach, and exhibited increases in neural activity a few seconds after the onset of the social approach (**Figure 4.1E**). Notably, during approaches to aggressors, correlations between neural activity and heart rate were not significantly different between the +HR and -HR encoders (**Figure 4.1F, bottom left**), indicating a decoupling between prefrontal neurocardiac networks and heart rate during this behavior. During avoidance of the CD1 aggressor, the activity of +HR encoders was significantly elevated relative to all neural populations, and the activity of -HR encoders was significantly reduced relative to all neural populations (**Figure 4.1C, right**). Once again, +HR encoders exhibited overall positive correlations with heart rate, which were larger (more positive) than those correlations between heart rate and -HR encoders (which were overall negative) (**Figure 4.1F, bottom right**). These results indicate that although

prefrontal neurocardiac networks can be activated during approaches to a threatening social stimulus, their ability to reliably track cardiac dynamics is diminished. This may reflect a context-dependent shift in prefrontal processing, in which interoceptive signals are temporarily down-weighted or disengaged during high-threat encounters, potentially to prioritize other survival-relevant computations such as threat assessment, decision-making, or escape preparation. Alternatively, high-threat encounters may involve heightened adrenergic activity – as observed with iso injections – that elevates sympathetic tone and suppresses interoceptive signaling.

**Neurocardiac encoding during NOE**

We next examined heart rate and prefrontal activity during NOE. Across mice, heart rate significantly increased during both approach and avoidance episodes compared to baseline, with the highest heart rates observed during approach episodes (**Figure 4.2B**). When directly comparing approach and avoidance episodes, heart rates were significantly higher during approaches (**Figure 4.2B**). These findings suggest that cardiac arousal during interaction with novel stimuli reflects the animal's ongoing behavior. The elevated heart rates observed during approach likely reflect heightened physiological arousal or exploratory engagement, whereas the increases during avoidance may represent more modest levels of physiological activation associated with withdrawal or disengagement.

To specifically evaluate how prefrontal neurocardiac networks track cardiac dynamics during NOE, we compared neural activity during approach and avoidance episodes toward the novel object. During approaches, +HR encoders significantly increased their

activity relative to all neural populations while -HR encoders exhibited no decrease in their activity relative to HR non-encoders (**Figure 4.2C, left**). Time-aligned analyses confirmed that +HR encoders exhibited sustained elevations in activity surrounding the onset of approach episodes, whereas -HR encoders exhibited sustained suppression (**Figure 4.2D**). The mean Pearson correlations between neural activity and heart rate during approaches did not significantly differ between +HR and -HR encoders (**Figure 4.2E, left**), suggesting that prefrontal neurocardiac networks become decoupled from heart rate during these periods.

In contrast, during avoidance episodes, the activity of +HR encoders was significantly elevated compared to all neural populations, and -HR encoders exhibited significantly decreased activity compared to all neural populations (**Figure 4.2C, right**). The mean Pearson's correlation between neural activity and heart rate during novel object avoidance episodes tended to be positive for +HR encoders and negative for -HR encoders, which had a mean correlation less than zero (**Figure 4.2E, right**), indicating reliable cardiac tracking by prefrontal networks during object avoidance.

Together these results demonstrate that prefrontal neurocardiac networks are actively engaged during NOE, and can maintain or lose their cardiac encoding based on the behavioral context. Overall, these findings highlight that prefrontal neurocardiac networks are not only sensitive not only to internal cardiac dynamics, but can also reconfigure in response to ongoing behavior, even in non-social and non-threatening contexts.

**Neurocardiac encoding during anxiety-related contexts**

We next assessed heart rate and prefrontal activity during anxiety-related avoidance behavior in the EPM. Across mice, heart rate significantly increased during time spent in the center, open, and closed arms of the maze compared to baseline (**Figure 4.3A**). Notably, heart rates were significantly higher in the open arms and center compared to the closed arms, consistent with increased physiological arousal in open environments commonly assumed to be more anxiogenic (**Figure 4.3A**). These results suggest that heart rate is dynamically modulated by environmental context, with center and open arm exposure eliciting heightened arousal relative to more sheltered regions of the maze.

To determine how prefrontal neurocardiac networks are modulated across distinct EPM zones, we compared neural activity across mPFC neural populations during center, open, and closed arm epochs. In the open arms, +HR encoders significantly increased their activity relative to -HR encoders, whereas -HR encoders were suppressed relative to all neural populations (**Figure 4.3B, left**). Interestingly, the activity of +HR encoders is not significantly different to the activity of HR non-encoders (**Figure 4.3B, left**). In the closed arms, +HR encoders significantly increased their activity relative to -HR encoders, whereas -HR encoders significantly decreased their activity relative to +HR encoders (**Figure 4.3B, middle**). The neural activity of +HR and -HR encoders exhibited no significant difference to the activity of HR non-encoders (**Figure 4.3B, middle**). In the center zone, +HR encoders exhibited significant increases in neural activity relative to all neural populations, while -HR encoders were significantly suppressed relative to +HR encoders (**Figure 4.3B, right**). These results suggest that

prefrontal networks are differentially engaged across EPM zones, with +HR encoders broadly active across contexts, -HR encoders consistently suppressed, and HR non-encoders showed context-dependent modulation, with greater engagement in the most anxiogenic zones such as the open arms.

To gain insight into how prefrontal neurocardiac networks dynamically respond to changes in anxiety-related context, we examined the temporal evolution of neural activity during EPM arm transitions – epochs in which the animal enters and exits the center zone. Time-locking neural activity to these transitions allowed us to capture rapid shifts in internal state as the animal approached or retreated from high-anxiety (open arms) to low-anxiety (closed arms) environments. Here, we aimed to determine whether divergence in activity between encoder types reflects the degree of emotional valence or exploratory drive during transitions. Rather than analyzing +HR and -HR encoders individually – which could obscure opposing trends due to noise and make it difficult to interpret the functional relationship between the two populations – we focused on the divergence in their activity to enhance sensitivity to their antagonistic dynamics. This differential measure provided a more robust index of network level encoding and may serve as a readout of internal state shifts relevant to threat appraisal and decision-making in anxiogenic contexts. During transitions which began and end in the same zone (open-to-open and closed-to-closed), the divergence in activity between +HR and -HR encoders increased after the transition point. Specifically, +HR encoders became more active, while -HR encoders showed further suppression, amplifying the divergence in their responses (**Figure 4.3C, top**). Notably, this increase in the activity divergence

was more pronounced during open-to-open transitions than closed-to-closed transitions, suggesting that the functional dissociation between +HR and -HR encoders is enhanced when the mouse engages in heightened exploratory behavior. When mice transitioned from the closed arms to the open arms (closed-to-open), the magnitude of this divergence is high before the transition but decrease following the transition, driven by suppression of +HR encoders and decrease in suppression of -HR encoders (**Figure 4.3C, bottom left**). In contrast, during transitions from the open arms into the closed arms (open-to-closed), the activity divergence between +HR and -HR encoders do not show a clear change before or after the transition (**Figure 4.3C, bottom right**). This suggests that divergence in prefrontal neurocardiac activity may serve as a predictive signal preceding transitions from low-anxiety into high-anxiety environment, but this divergence is diminished once the animal enters the high-anxiety context – whereas transitions from high-anxiety into low-anxiety environment are not preceded by such predictive dynamics, and divergence remains stable once the animal enters the low-anxiety context. Quantifying the mean change in z-score pre- versus post-transition confirmed these bidirectional modulations across all four transition types (**Figure 4.3D**). To further characterize the functional dissociation between +HR and -HR encoders across EPM zones, we computed the Pearson correlation between each neuron's activity and heart rate during closed, center, and open arm epochs. Overall, correlation values across all EPM zones were positive for +HR encoders and negative for -HR encoders, with a significant difference between the two populations. +HR encoders showed the highest positive correlation with heart rate in the closed arms, with a modest but still significant correlation in the open arms (**Figure 4.3E**). In contrast, -HR encoders

exhibited the most negative correlations in the closed arms, with correlations becoming less negative in the open arms (**Figure 4.3E**). These patterns suggest that neurocardiac tuning is strongest in the closed arms and diminishes in the open arms for both +HR and -HR encoders. In the center zone, the difference in correlation values between +HR and -HR encoders was not statistically significant (**Figure 4.3E**), suggesting weaker or more variable neurocardiac encoding in this transitional and anxiogenic region of the maze. These findings indicate that prefrontal neurocardiac representations are differentially modulated by environmental context, with stronger and more polarized heart rate encoding in behaviorally less anxiogenic zones and weaker encoding in high anxiogenic zone.

## 4.4 Discussion

In this study, we used simultaneous single-cell calcium imaging and ECG recordings in freely moving mice to investigate how prefrontal neurocardiac networks dynamically encode heart rate across a range of naturalistic behaviors. By tracking neural and cardiac dynamics during social interactions, NOE, and anxiety-related navigation in the EPM, we identified distinct populations of mPFC neurons that flexibly couple to internal cardiac states. These networks were not static encoders but dynamically modulated their activity and coupling strength in a behavior- and context-dependent manner, adapting to the motivational valence and arousal demands of the environment.

During social exploration, we observed that heart rate was not only elevated during both approach and avoidance behaviors but was also shaped by the type of social target and

behavioral strategy. Notably, anticipatory arousal – quantified by changes in heart rate – was greatest during approach to the juvenile conspecific, whereas defensive arousal – also quantified by changes in heart rate – peaked during avoidance of the CD1 aggressor. While both of these behaviors were arousing, as measured by the change in heart rate, they engaged prefrontal neurocardiac networks in different ways. During juvenile approach, +HR encoders increased and -HR encoders decreased their activity in a sustained, time-locked manner. Heart rate was reliably encoded by these networks during this behavior, with overall positive correlations in the +HR encoder population vs. negative correlations in the -HR encoder population.

In contrast, approach to the CD1 aggressor was marked by elevated activity in +HR encoders and increased neural activity of -HR encoders following approach, yet these responses did not correlate with persistent encoding of heart rate, indicating a functional decoupling between neural and cardiac signals. This disruption in neurocardiac coupling may reflect a transient disengagement of interoceptive processing when attentional and motor systems are redirected toward external threat cues or due to elevated adrenergic activity – as seen with iso injections – that increases sympathetic tone and blunts interoceptive processing. However, during CD1 avoidance, neurocardiac tracking re-emerged: both +HR and -HR encoders showed significant correlations with heart rate, suggesting that these networks re-engage to support internal monitoring during behavioral withdrawal. These results highlight that prefrontal neurocardiac networks are sensitive to the interplay between social threat, behavioral choice, and physiological state, flexibly adjusting their encoding to match the demands of the moment.

Similar flexibility was observed during NOE. Here, heart rate was highest during approach, consistent with exploratory arousal, and lower (but still elevated) during avoidance. +HR and -HR encoders responded robustly during approach, but these populations no longer encoded heart rate in a consistent manner. In contrast, avoidance episodes elicited more stereotyped responses: +HR encoders maintained overall positive correlations, -HR encoders remained overall negatively correlated. These results suggest that during exploration of a novel object, neurocardiac networks may transiently reshape their encoding to balance internal and external information about a potentially threatening object, whereas during avoidance, they may adopt a more stable encoding pattern to support sustained arousal regulation after disengaging from an object deemed no longer threatening.

In the EPM, neurocardiac encoding was further modulated by environmental anxiety. Heart rate was elevated across all maze zones but highest in the center and open arms, where mice experience greater exposure and risk. +HR encoders were activated and -HR encoders suppressed across all regions, but the divergence in their activity levels and their correlation with heart rate varied by zone. The strongest and most polarized encoding occurred in the closed arms, a relatively low-anxiety environment, where both populations showed maintained coupling to heart rate. In the open arms and center zone, encoding diminished for both +HR and -HR encoders, with overall correlation values across each population approaching zero. These patterns suggest that interoceptive tracking by the mPFC is most robust in low-anxiety contexts and

selectively reduced during high-anxiety exposure, potentially to allocate cognitive resources toward external monitoring and decision-making.

Transitions between EPM zones further revealed dynamic reorganization of neurocardiac encoding. Continuous occupancy in a single zone led to greater divergence between +HR and -HR encoders, particularly during open-to-open transitions (suggesting enhanced interoceptive tuning during heightened exploratory behavior). Conversely, transitions from a low-anxiety context into a high anxiety-context (e.g., closed-to-open) led to decreases in activity divergence between +HR and -HR encoders. These dynamics may reflect a transient reorganization of prefrontal activity during decision-making. For example, as mice prepare to transition into anxiogenic zones, mPFC activity may become dominated by computations related to threat assessment or behavioral selection, temporarily overriding interoceptive encoding. Alternatively, transitions into anxiogenic contexts might occur during periods when interoceptive monitoring is downregulated, thereby facilitating exploratory behavior despite potential internal conflict.

Together, our results reveal that mPFC neurocardiac networks dynamically track heart rate across diverse behavioral contexts, adjusting their activity and coupling strength in line with internal arousal and motivational state. These networks exhibit flexible, context-specific engagement: they strengthen interoceptive encoding during low social threat contexts and object avoidance, disengage during high-threat confrontation, and reorganize dynamically as animals navigate complex environments. This functional versatility suggests that prefrontal neurocardiac networks contribute to the integration of

physiological state with behavior, enabling the brain to adaptively regulate responses based on both internal and external cues.

While our findings provide compelling evidence for dynamic neurocardiac encoding across behavioral contexts, several limitations should be considered. First, calcium imaging inherently has slower temporal resolution compared to electrophysiology, which may have limited our ability to detect rapid or transient changes in neural activity that more precisely track beat-to-beat fluctuations in heart rate. Second, while we interpret correlation-based metrics as indices of neural-cardiac coupling, these relationships are associative and do not imply causality. It remains unclear whether +HR or -HR encoders directly influence cardiac output, receive afferent input from cardiovascular signals, or track another internal variable that co-varies with heart rate. Third, our behavioral classification of “approach” and “avoidance” is based on proximity and directionality, which, while meaningful, may not capture the full landscape of internal motivational states or affective processing. Finally, although we categorized different areas of the EPM as separate behavioral states, anxiety-related decision making may occur more gradually and in a nuanced and multifaceted manner. Animals may experience shifting levels of stress or uncertainty as they move through the maze, which could make it harder to clearly define distinct zones associated with characteristic neural and cardiac responses.

These findings have important implications for our understanding of interoception and its role in adaptive behavior. By demonstrating that the prefrontal cortex contains functionally distinct neuronal populations that track heart rate in a context-dependent

manner, this work provides a framework for exploring how disruptions in interoceptive encoding might contribute to maladaptive states such as anxiety, hypervigilance, or social withdrawal. Future studies using causal manipulations of +HR and -HR encoders could clarify whether these networks merely monitor cardiac signals or actively shape physiological and behavioral responses. Moreover, longitudinal tracking of these networks under chronic stress or in disease models may uncover how neurocardiac encoding is altered in affective disorders. Finally, integrating these signals with closed-loop behavioral paradigms could offer new insight into how internal state representations guide real-time decision-making and behavior.

## 4.5 Figures

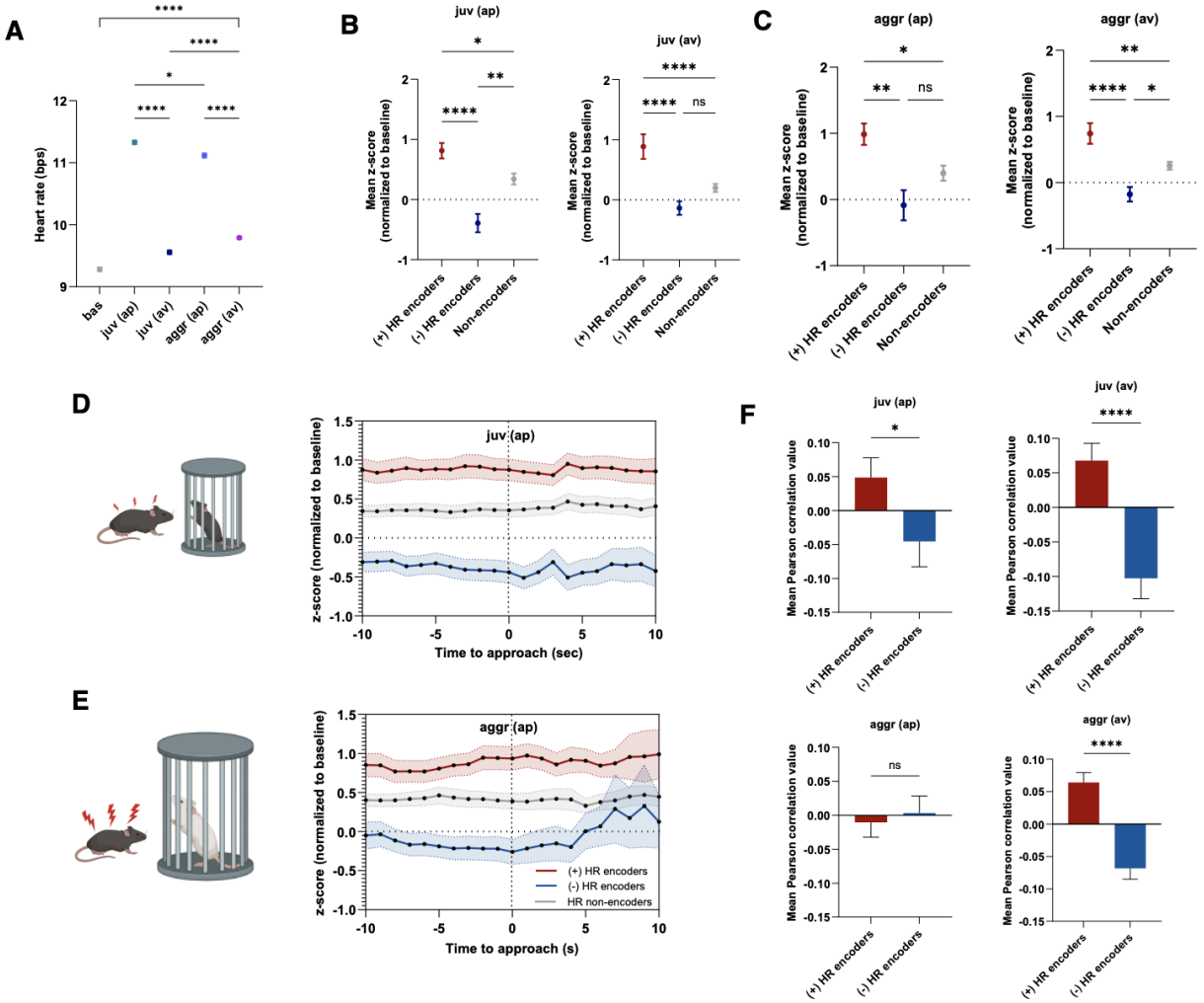


**Figure 4.1. Prefrontal neurocardiac networks in social behaviors.** (A) Mean heart rate during baseline (bas), approach (ap) and avoidance (av) of a juvenile conspecific (juv) or CD1 aggressor (aggr). (B) Mean z-scored activity of +HR encoders, -HR encoders, and HR non-encoders during juvenile approach (*left*) (n = 8 mice, 644 neurons) and juvenile avoidance (*right*) (n = 5 mice, 413 neurons). (C) Same as (B), but during approach (n = 8 mice, 644 neurons) and avoidance (n = 8 mice, 644 neurons) of the CD1 aggressor. (D) *Left*, Schematic of the juvenile interaction assay. *Right*, Time-aligned activity of HR encoders during approach to the juvenile (time 0 = entry into approach zone). (E) *Left*, Schematic of the aggressor interaction assay. *Right*, Time-aligned activity of HR encoders during approach to the CD1 aggressor. (F) Mean Pearson correlation between HR encoder activity (DF/F) and heart rate during approach (*left*) and avoidance (*right*) for both juvenile (*top*) and CD1 aggressor (*bottom*) conditions. Data represent mean ± SEM. *$p < 0.05$, **$p < 0.01$, ****$p < 0.0001$; ns = not significant.

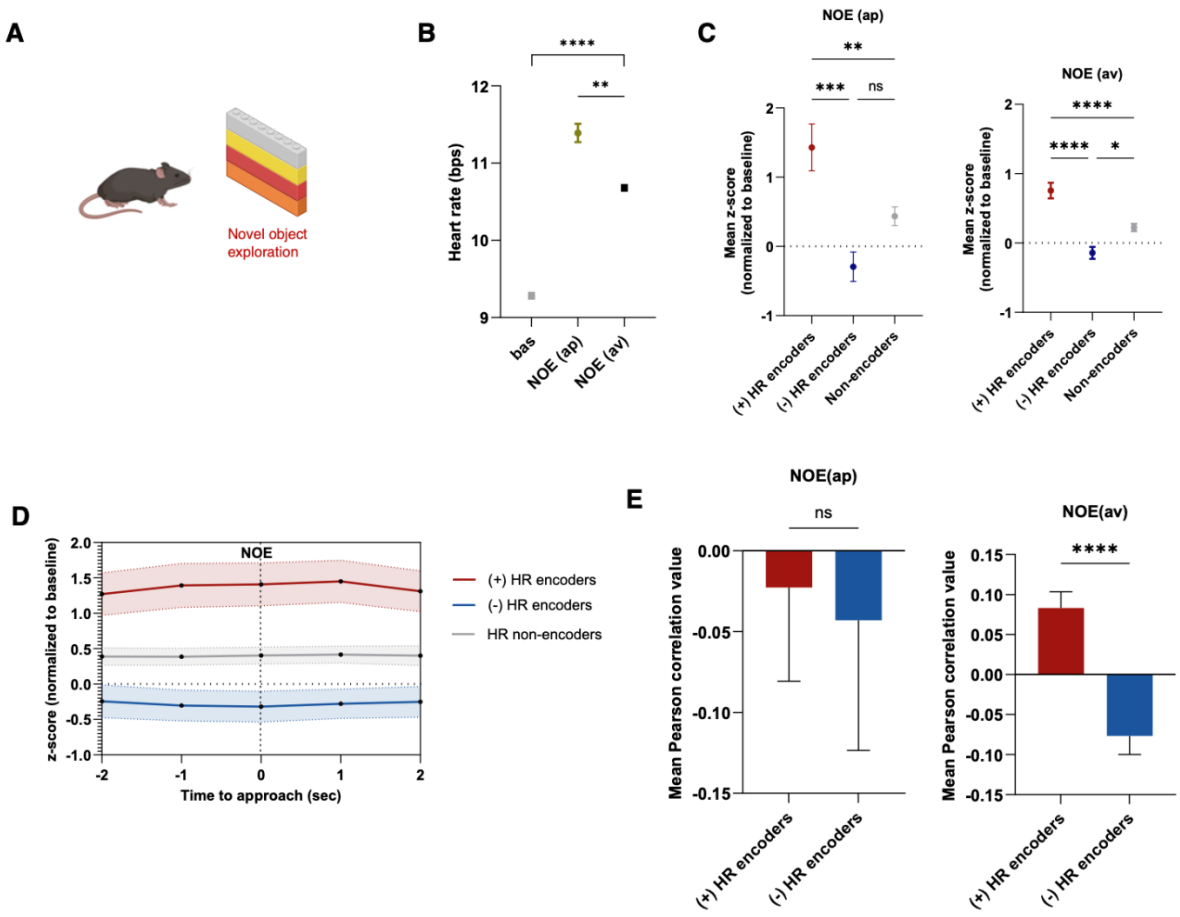


**Figure 4.2. Prefrontal neurocardiac networks during novel object exploration.** (A) Schematic of the NOE paradigm. (B) Mean heart rate during baseline (bas), novel object approach (ap) (n = 6 mice, 464 neurons), and avoidance (av) (n = 8 mice, 644 neurons). (C) Mean z-scored calcium activity of +HR encoders, -HR encoders, and HR non-encoders during approach (*left*) and avoidance (*right*) of the novel object. (D) Time-aligned average activity of each neural population during approach to the novel object (time 0 = approach onset). (E) Mean Pearson correlation between neural activity (DF/F) and heart rate for +HR and -HR encoders during novel object approach (*left*) and avoidance (*right*). Data represent mean ± SEM. *$p < 0.05$, **$p < 0.01$, ***$p < 0.001$, ****$p < 0.0001$; ns = not significant.

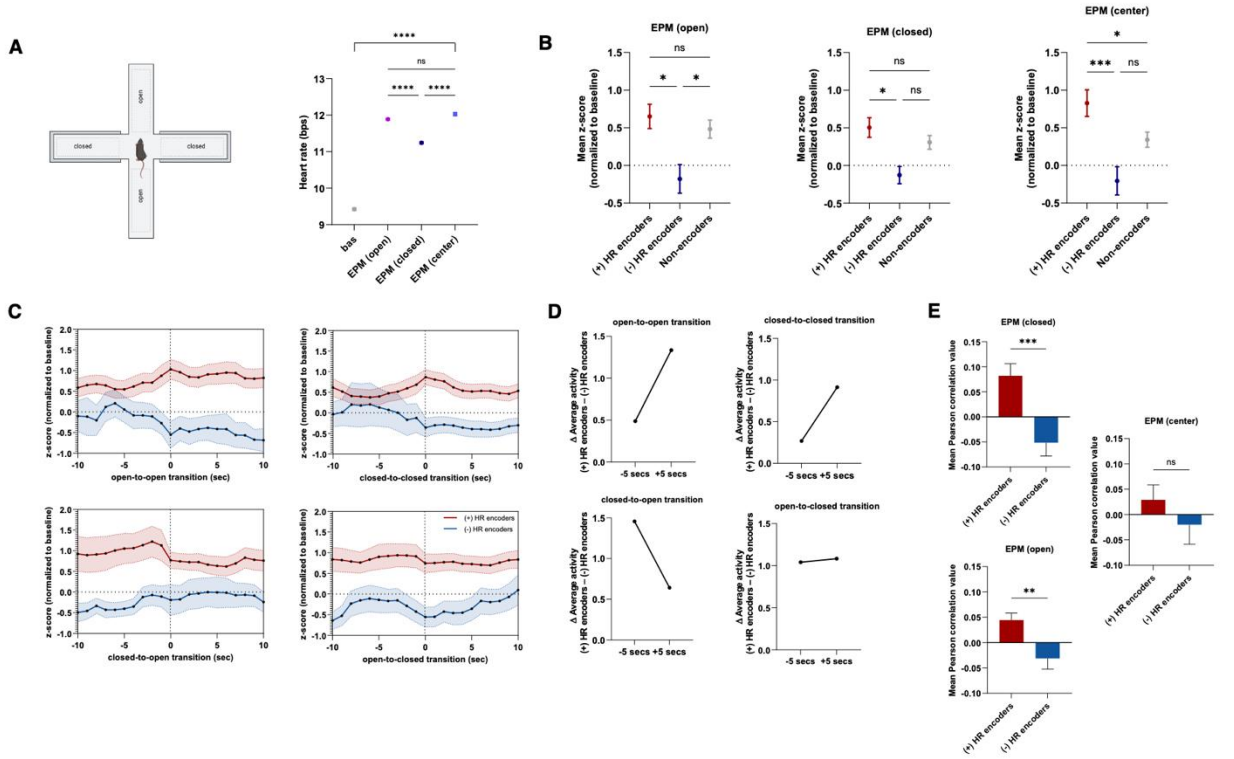


**Figure 4.3. Prefrontal neurocardiac networks in anxiety behaviors.** (A) Left, Schematic of the EPM with open and closed arms. *Right*, Mean heart rate during baseline (bas) and while the mouse is in the open arms, closed arms, and center zone. (B) Mean z-scored activity of +HR encoders, -HR encoders, and HR non-encoders during time spent in the open arms (n = 6 mice, 437 neurons), closed arms (n = 6 mice, 437 neurons), and center zone (n = 6 mice, 437 neurons). (C) Time-aligned population activity (z-score in 1-second bins) of +HR and -HR encoders during arm transitions (time 0 = transition point). Open-to-open (n = 4 mice, 289 neurons) denotes transition from one open arm into the other open arm; closed-to-closed (n = 5 mice, 356 neurons) denotes transition from one closed arm into the other closed arm; closed-to-open (n = 5 mice, 381 neurons) denotes transition from closed arm into open arm; open-to-closed (n = 6 mice, 437 neurons) denotes transition from open arm into closed arm. (D) Change in activity (difference in z-score) between +HR and -HR encoders, calculated by comparing neural activity at -5 and +5 seconds relative to EPM transitions. (E) Mean Pearson correlation between HR encoder activity (DF/F) and heart rate across EPM zones. Data represent mean ± SEM. *$p < 0.05$, **$\mathbf{p} < 0.01$, ***$\mathbf{p} < 0.001$, ****$\mathbf{p} < 0.0001$; ns = not significant.

## 4.6 References


1. Livermore, J. J., Klaassen, F. H., Bramson, B., Hulsman, A. M., Meijer, S. W., Held, L., ... & Roelofs, K. (2021). Approach-avoidance decisions under threat: the role of autonomic psychophysiological states. *Frontiers in Neuroscience*, *15*, 621517.
2. Klaassen, F. H., de Voogd, L. D., Hulsman, A. M., O'Reilly, J. X., Klumpers, F., Figner, B., & Roelofs, K. (2024). The neurocomputational link between defensive cardiac states and approach-avoidance arbitration under threat. *Communications Biology*, *7*(1), 576.
3. Van Den Buuse, M., Van Acker, S. A., Fluttert, M., & De Kloet, E. R. (2001). Blood pressure, heart rate, and behavioral responses to psychological "novelty" stress in freely moving rats. *Psychophysiology*, *38*(3), 490-499.
4. Dinç, F., Inan, H., Hernandez, O., Schmuckermair, C., Hazon, O., Tasci, T., ... & Schnitzer, M. J. (2021). Fast, scalable, and statistically robust cell extraction from large-scale neural calcium imaging datasets. *BioRxiv*, 2021-03.
5. Corder, G., Ahanonu, B., Grewe, B. F., Wang, D., Schnitzer, M. J., & Scherrer, G. (2019). An amygdalar neural ensemble that encodes the unpleasantness of pain. *Science*, *363*(6424), 276-281.

**Publishing Agreement**

It is the policy of the University to encourage open access and broad distribution of all theses, dissertations, and manuscripts. The Graduate Division will facilitate the distribution of UCSF theses, dissertations, and manuscripts to the UCSF Library for open access and distribution. UCSF will make such theses, dissertations, and manuscripts accessible to the public and will take reasonable steps to preserve these works in perpetuity.

I hereby grant the non-exclusive, perpetual right to The Regents of the University of California to reproduce, publicly display, distribute, preserve, and publish copies of my thesis, dissertation, or manuscript in any form or media, now existing or later derived, including access online for teaching, research, and public service purposes.

DocuSigned by:
Gabriel Mateo Semidey
A494DAE0A084418...
Author Signature

8/1/2025
Date